MAXWELL
S-CUBED Division

SSS-TR-91-12833

Two-Dimensional Axisymmetric Calculations of Surface Waves Generated by an Explosion in an Island, Mountain and Sedimentary Basin

J. L. Stevens
K. L. McLaughlin
S. M. Day
B. Shkoller

Technical Report

Sponsored by:
DEFENSE ADVANCED RESEARCH PROJECTS AGENCY (DoD)

Monitored by:
U.S. AIR FORCE TECHNICAL APPLICATIONS CENTER
Under Contract No. F08606-89-C-0022

October 1991

P. O. Box 1620, La Jolla, California 92038-1620
(619) 453-0060

REPORT DOCUMENTATION PAGE

Form Approved
OMB No. 0704-0188

1. AGENCY USE ONLY *(Leave blank)*	2. REPORT DATE	3. REPORT TYPE AND DATES COVERED
	October 1991	Technical Report

4. TITLE AND SUBTITLE
Two-Dimensional Axisymmetric Calculations of Surface Waves Generated by an Explosion in an Island, Mountain and Sedimentary Basin

5. FUNDING NUMBERS
C - F08606-89-C-0022

6. AUTHOR(S)
J. L. Stevens, K. L. McLaughlin, S. M. Day, and B. Shkoller

7. PERFORMING ORGANIZATION NAME(S) AND ADDRESS(ES)
S-CUBED, A Division of Maxwell Laboratories, Inc.
P.O. Box 1620
La Jolla, CA 92038-1620

8. PERFORMING ORGANIZATION REPORT NUMBER
SSS-TR-91-12833

9. SPONSORING/MONITORING AGENCY NAME(S) AND ADDRESS(ES)
Defense Advanced Research Projects Agency
3701 N. Fairfax, Suite 717
Arlington, VA 22209-1714

10. SPONSORING/MONITORING AGENCY REPORT NUMBER

11. SUPPLEMENTARY NOTES

12a. DISTRIBUTION/AVAILABILITY STATEMENT
Unlimited Distribution

12b. DISTRIBUTION CODE

13. ABSTRACT *(Maximum 200 words)*

The generation of long period (20-50 second) surface waves by an explosion on an island, inside a mountain, or near a material discontinuity is studied using two-dimensional axisymmetric finite difference calculations. The generation of surface waves can be reduced substantially if the explosion is close to a vertical boundary such as a material velocity reduction, mountain slope, or island/ocean boundary. This occurs because the horizontal components of the static stress field are reduced at the boundary.

Three sets of finite difference calculations were performed for an "island" surrounded by an "ocean" of air, water and a low velocity solid. Calculations include "ocean" depths of 3 km and 6 km, and the "island" varies in diameter from 6 km to 48 km. For a 48 km island material boundary has little effect on the surface waves. For an island width equal to the ocean depth, however, the surface wave generation is reduced by an order of magnitude for air and water, and reduced by more than a factor of 2 for the low velocity

14. SUBJECT TERMS		15. NUMBER OF PAGES
Surface Waves	Explosion Seismology	36
Finite Difference	Novaya Zemlya	16. PRICE CODE
Amchitka	Mururoa	

17. SECURITY CLASSIFICATION OF REPORT	18. SECURITY CLASSIFICATION OF THIS PAGE	19. SECURITY CLASSIFICATION OF ABSTRACT	20. LIMITATION OF ABSTRACT
Unclassified	**Unclassified**	**Unclassified**	

CLASSIFIED BY:

DECLASSIFY ON:

13. Abstract (Continued)

solid. Comparisons with the geography of the Amchitka and Mururoa island test sites show that this effect is small for explosions at those sites, however the effect appears to be important for Novaya Zemlya and other sites where explosions are detonated inside mountains, and at sites with strong material variations. A similar numerical experiment for an explosion in a sedimentary basin shows that surface waves can be amplified by the presence of a high velocity non-source boundary.

TABLE OF CONTENTS

LIST OF ILLUSTRATIONS

LIST OF ILLUSTRATIONS (Continued)

SUMMARY

The generation of long period (20-50 second) surface waves by an explosion on an island, inside a mountain, or near a material discontinuity is studied using two-dimensional axisymmetric finite difference calculations. The generation of surface waves can be reduced substantially if the explosion is close to a vertical boundary such as a material velocity reduction, mountain slope, or island/ocean boundary. This occurs because surface waves from a shallow explosion are generated primarily by the horizontal stress components which are reduced at the boundary.

Three sets of finite difference calculations were performed for an "island" surrounded by an "ocean" of air, water, and a low velocity solid. The surface waves are measured on "land" on the other side of the "ocean." A "solid" calculation with a uniform structure is also performed for comparison. Calculations include "ocean" depths of 3 km and 6 km, and the "island" varies in diameter from 6 km to 48 km. For a 48 km island, the material boundary has little effect on the surface waves. For an island width equal to the ocean depth, however, the surface wave generation is reduced by an order of magnitude for air and water, and reduced by more than a factor of 2 for the low velocity solid. Comparisons with the geography of the Amchitka and Mururoa island test sites show that this effect is small for explosions at those sites, however the effect appears to be important for Novaya Zemlya and other sites where explosions are detonated inside mountains, and at sites with strong material variations.

To estimate the effect of a high velocity boundary surrounding a low velocity source region, we performed a calculation for an explosion in a sedimentary basin modeled after Yucca Valley at the Nevada Test Site. In order to include finer details of the source region, a finely gridded finite difference calculation was performed in the source region, and surface waves exterior to the calculation were calculated using the representation theorem. We find that surface waves are amplified by about a factor of two by the high velocity interface surrounding the low velocity valley.

1. INTRODUCTION

We investigate the effect of a near-source boundary or material property change on the generation of long period surface waves by explosions. This work was initially motivated by the work of von Seggern (1978), and others who found a possible bias between Amchitka and NTS and suggested that surface waves generated by an explosion on an island might differ from those generated by a mid-continent explosion. The surface wave amplitudes from the Amchitka explosion Milrow, for example, were significantly lower than the surface wave amplitudes for the NTS explosions Boxcar, Benham, and Handley, all of which had similar yields (von Seggern, 1978; Stevens, 1986b). Earlier investigations have looked at the effect of tectonic release (Toksoz and Kehrer, 1972) and large scale three-dimensional earth structure (McLaughlin, *et al*, 1991).

There is a common perception that surface waves should not be affected strongly by the details of the source region, because surface waves are long period phenomena with wavelengths much larger than a test site. However, surface waves exist because of the free surface boundary condition, and changes in the boundary shape can affect surface wave generation. This is particularly true for explosions, because long period surface waves from explosions are generated by the static horizontal stress field that remains after the explosion has been detonated. If the stress field is relieved by the presence of a vertical boundary such as an island/ocean interface or the side of a mountain, then the long period surface waves can be sharply reduced, even though the scale of the structural changes are much smaller than a wavelength. In addition to Amchitka, the French nuclear test site at Mururoa is located on an island that drops very steeply into the South Pacific ocean. At the old French Sahara test site and the two Soviet test sites at Novaya Zemlya and Degelen Mountain, explosions are detonated inside mountains.

We have performed a series of finite difference calculations to model the effect of the island/ocean interface on explosion-generated surface waves. "Island" is used here in a generic sense to mean a source region of higher velocities than the surrounding regions. We have performed three sets of calculations: first with the island surrounded by air; second with the island

surrounded by water; and third with the island surrounded by a low velocity solid. The calculations therefore apply not only to an explosion on an island, but also to an explosion in a mountain, or to an explosion in a high velocity intrusion such as a salt plug surrounded by low velocity sediments. We look in particular at the effect of the size of the island and the depth of the ocean on the surface wave amplitudes. We show in the following sections that the surface wave amplitudes can be reduced significantly by the presence of a vertical boundary near the source.

The calculations described above were performed with a fairly coarse grid spacing in order to directly calculate surface waves several hundred kilometers from the explosion. In order to better quantify the effect of depth on surface wave generation, we also performed a series of plane strain calculations of the dilatation at several depths due to a Rayleigh wave incident on a mountain and then used reciprocity to determine the effect of depth on Rayleigh wave generation by explosions at these depths. We find that the Rayleigh wave amplitude is reduced significantly, even for an explosion at the base of the mountain, and is strongly reduced for explosions within the mountain.

We also performed an axisymmetric calculation of an explosion in a mountain modeled after a profile of a mountain at the Novaya Zemlya test site. In this case, we used a much more finely gridded model than in the calculations discussed above and used the representation theorem to generate surface waves at distances outside the grid. This was done by saving the displacements and stresses on a monitoring surface in the exterior structure and then integrating together with a multi-modal surface wave Green's function to generate surface waves. Explosions were located within the mountain and just below the base of the mountain. The results agree with the plane strain reciprocal experiment discussed above. The surface wave amplitudes are reduced, and reduced substantially more for the explosion within the mountain.

We investigate the effect of a high velocity boundary on the generation of surface waves by an explosion in a low velocity medium. A two-dimensional model was developed for Yucca Valley at the Nevada Test Site, which is a region of low velocity sediments surrounded by higher velocity rock. The

calculation used a finely gridded source region and used the representation theorem to generate surface waves, as with the Novaya Zemlya mountain calculation. The resulting surface waves were compared with synthetic seismograms generated by an explosion in a plane-layered structure corresponding to the structure at the source and then propagating into the external plane-layered structure, using a transmission coefficient based on conservation of energy. In this case, we find that the Rayleigh wave amplitudes are substantially enhanced by the high velocity boundary.

2. ISLAND/OCEAN FINITE DIFFERENCE CALCULATIONS

All calculations were performed with the two-dimensional axisymmetric finite difference code TRES-2D running on a CRAY 2 supercomputer. The explosion was modeled as an isotropic moment tensor source with a time function proportional to $\alpha^2 te^{-\alpha t}$, α = 0.1 Hz (corresponding to a minimum phase source with corner frequency at 0.1 Hz). The source was converted to a pressure applied to two vertical zones on the axis of symmetry. The source is therefore shaped as a cylinder with equal height and radius, and is approximately isotropic. For the series of island/ocean calculations, we used a uniform grid spacing of 1.5 km, which is designed to allow accurate resolution of surface waves in the 20-50 second period band. The source was located immediately below the free surface. A schematic diagram of the geometry used in the calculations is shown in Figure 1. Calculations were performed for island radii ranging from 3 km to 24 km and for ocean depths of 3 km and 6 km.

The "ocean" in this model is a region with material properties different from the background model. The background model is a plane-layered model (listed in Table 1) and is equivalent to a north-south cross-section near the Amchitka test site in the three dimensional model of McLaughlin, *et al.* (1991). One calculation was performed as a reference using the background structure without the ocean. Three sets of calculations were performed with different material models in the "ocean." In the first set of calculations, the ocean was filled with water using standard water density and compressional velocity. In the second set of calculations, a free surface boundary condition was used on the bottom and sides of the ocean, thus simulating air or vacuum in the "ocean." In the third set of calculations, the ocean was filled with a solid with a compressional velocity of 2.4 km/sec, a shear velocity of 1.3 m/sec, and a density of 1.9 g/cm^3. These values are typical of the volcanic tuffs found at the Nevada Test Site. This model therefore simulates a high velocity intrusion into a lower velocity medium.

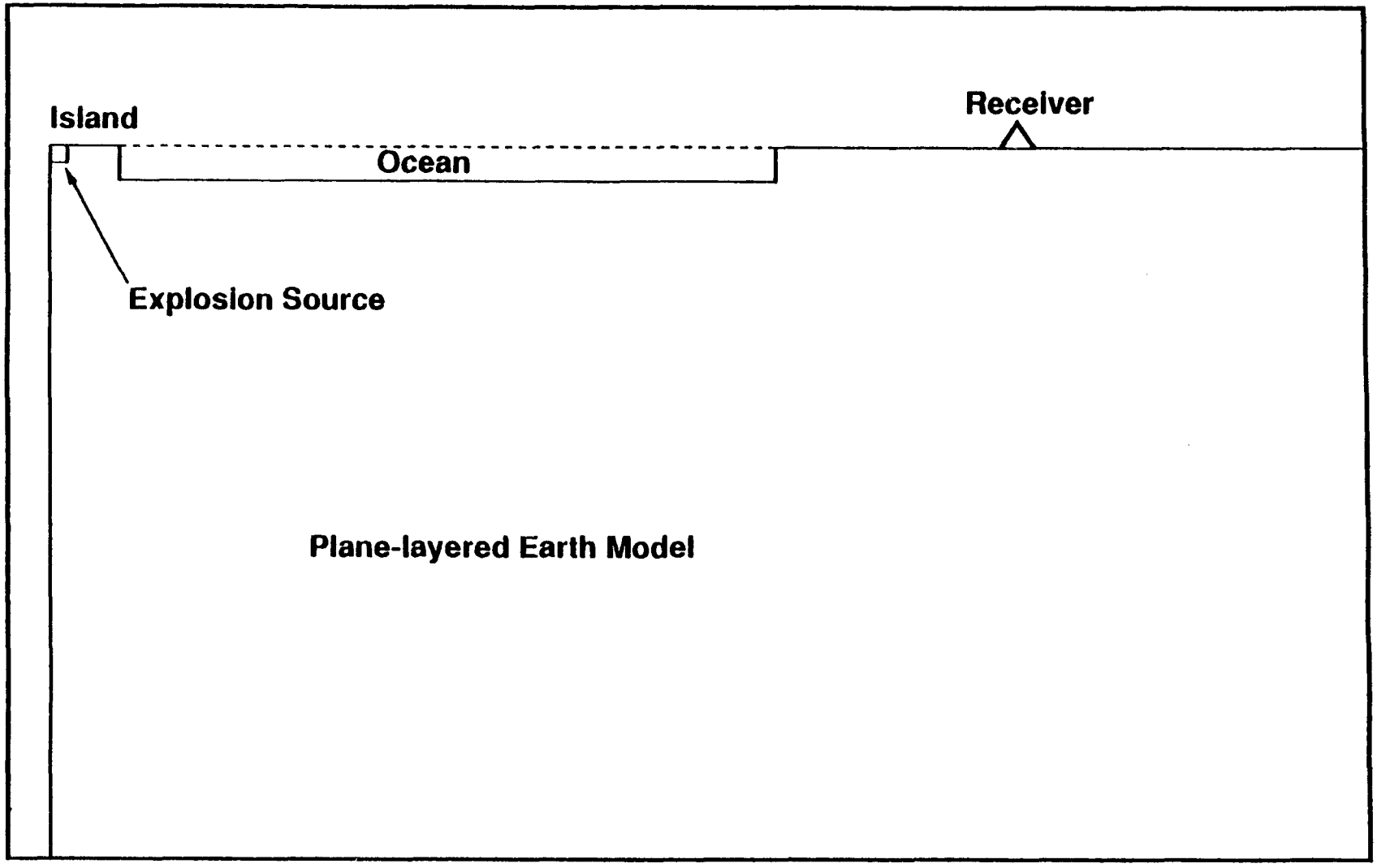

Figure 1. Geometry of the two-dimensional axisymmetric finite difference calculations. The explosion source is located just below the surface at the origin. The ocean extends to a distance of 354 km from the origin, and the receiver is located 390 km from the origin. The set of calculations includes ocean depths of 3 km and 6 km, and island radii ranging from 3 km to 24 km.

Table 1
Background Structure for the Axisymmetric Calculations

Depth km	Thickness km	P-Velocity km/sec	S-Velocity km/sec	Density gm/cc
6.0	6.0	6.90	3.90	2.29
18.0	12.0	6.90	3.90	2.29
54.0	36.0	8.00	4.50	3.30
78.0	24.0	8.00	4.45	3.30
126.0	48.0	8.00	4.40	3.25
150.0	24.0	8.04	4.40	3.37
186.0	36.0	8.02	4.40	3.37
222.0	36.0	8.01	4.40	3.36
258.0	36.0	8.60	4.66	3.45
294.0	36.0	8.65	4.68	3.46
330.0	36.0	8.73	4.70	3.49
366.0	36.0	8.79	4.73	3.51
402.0	36.0	8.87	4.76	3.53
∞	∞	9.15	4.95	3.73

In Figure 2, we show the seismograms calculated for the uniform background model together with seismograms for the 1.5 km and 3 km source in a 6 km radius/6 km high island surrounded by air at a distance of 390 km from the source. The seismograms differ substantially in amplitude, with the island seismograms lower in amplitude than the background seismogram.

In order to examine the frequency dependence of the seismograms, the amplitude and phase of the surface waves at the receiver were recovered by narrow band filtering and phase-matched filtering as described by Stevens (1986a). The source function was deconvolved during the processing, so the spectra correspond to a source with a step function in moment. In Figure 3, we show the spectra between .01 and 0.1 Hz for the uniform background structure, and for the water, air, and solid filled ocean cases with an island radius of 24 km, and an ocean depth of 3 km. For this small aspect ratio (aspect ratio is defined here to be the ratio of the island height to the island radius), the island structure has little effect on the surface wave amplitudes. The material property

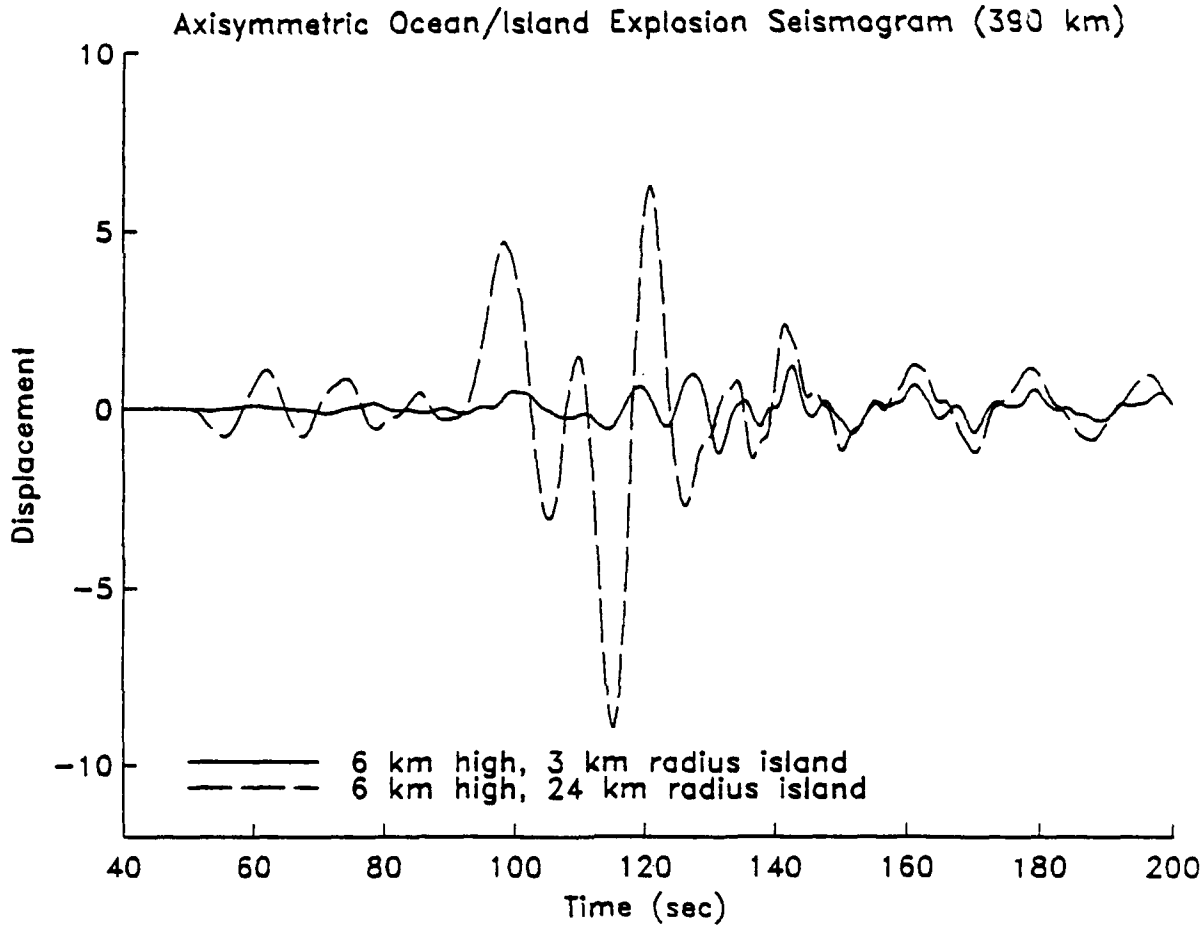

Figure 2. Seismograms at a range of 390 km for the 3 km radius and 24 km radius, 6 km high island. The surface wave is reduced dramatically for the source in the small island.

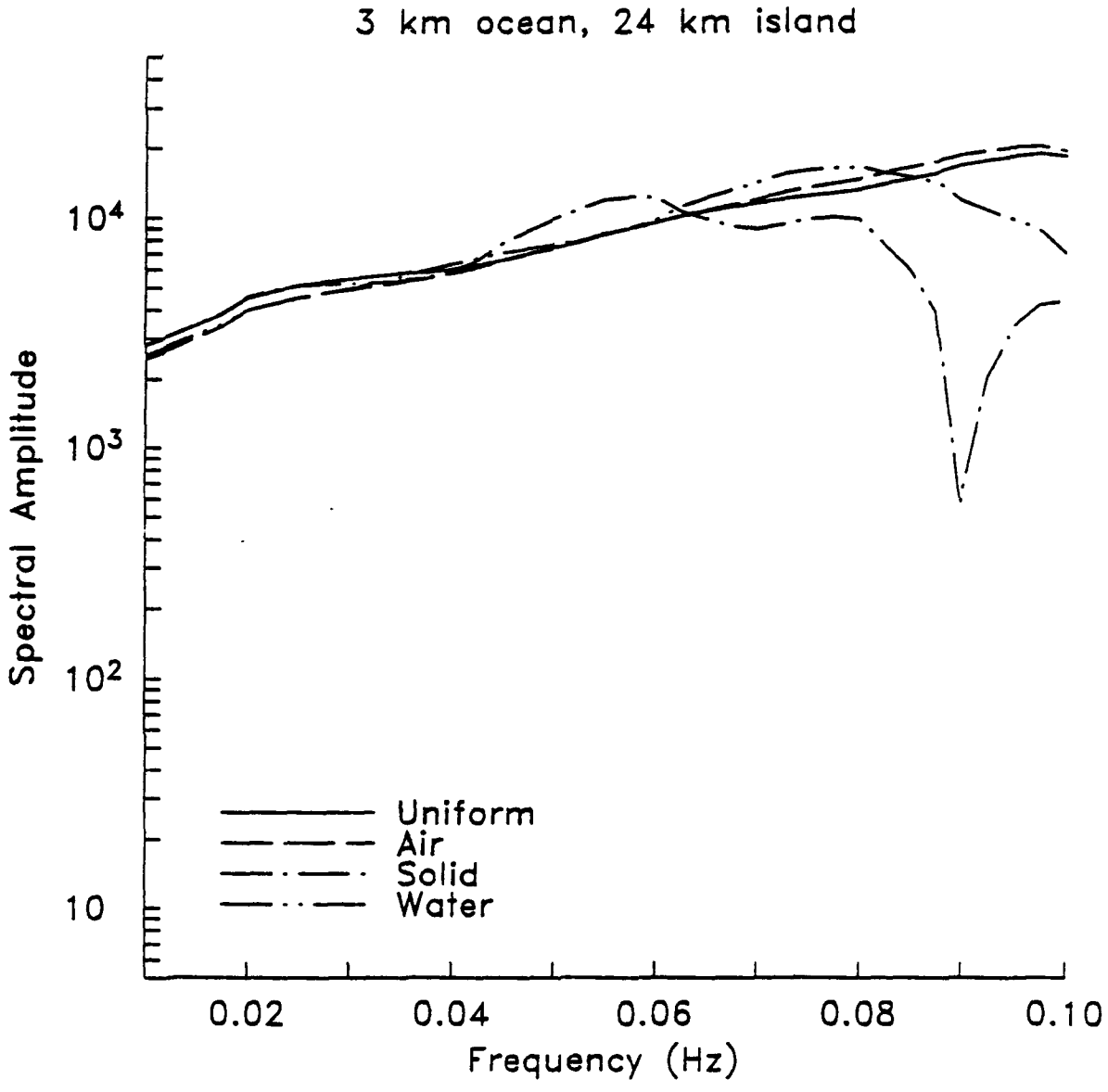

Figure 3. Spectra of surface waves recorded at 390 km from a 24 km radius island across the uniform background structure, and across an "ocean" filled with water, air, and a lower velocity solid. In each case, the "ocean" is 3 km deep. The "ocean" material has some effect on shorter period surface waves, but there is little difference between the three cases at periods greater than 20 seconds.

differences cause some variation in spectral amplitude at higher frequencies, but at frequencies less than 0.05 Hz, there is very little difference between the surface wave amplitudes for any of the four structures.

In Figure 4, we show the surface wave amplitudes for an island radius of 6 km and an ocean depth of 6 km. In this case the amplitudes are very strongly reduced for all three ocean types. At 25 second period (0.04 Hz), the amplitudes are reduced relative to the uniform case by factors of 2, 6, and 20 for the solid, water, and air filled ocean cases, respectively. In Figures 5, 6, and 7, we show the 25 second amplitude as a function of the aspect ratio of the island. In each case, the amplitude is reduced for aspect ratios greater than about 0.2, and the amplitudes are reduced by a factor of 2 at aspect ratios of 0.35, 0.4, and 0.7 for air, water, and solid, respectively. For the solid model used here, the amplitude is reduced by a maximum of about a factor of 2.5, but the amplitude reduction can be much larger for the air and water cases.

In Figure 8, we show the bathymetry near the Amchitka and Mururoa test sites. The Amchitka bathymetry was derived by drawing a line southwest from the test site using maps from Olsen, *et al.* (1972). The Mururoa bathymetry was derived similarly by drawing a line to the northwest of the test site using maps from DMA (1983). For Amchitka, the aspect ratio is only about 0.05, so clearly the amplitude reduction from the island structure at Amchitka is negligible. At Mururoa, however, the ocean drops off much more quickly away from the test site, and the aspect ratio of the island is approximately 0.25. So surface waves might be reduced slightly at the Mururoa test site by this effect.

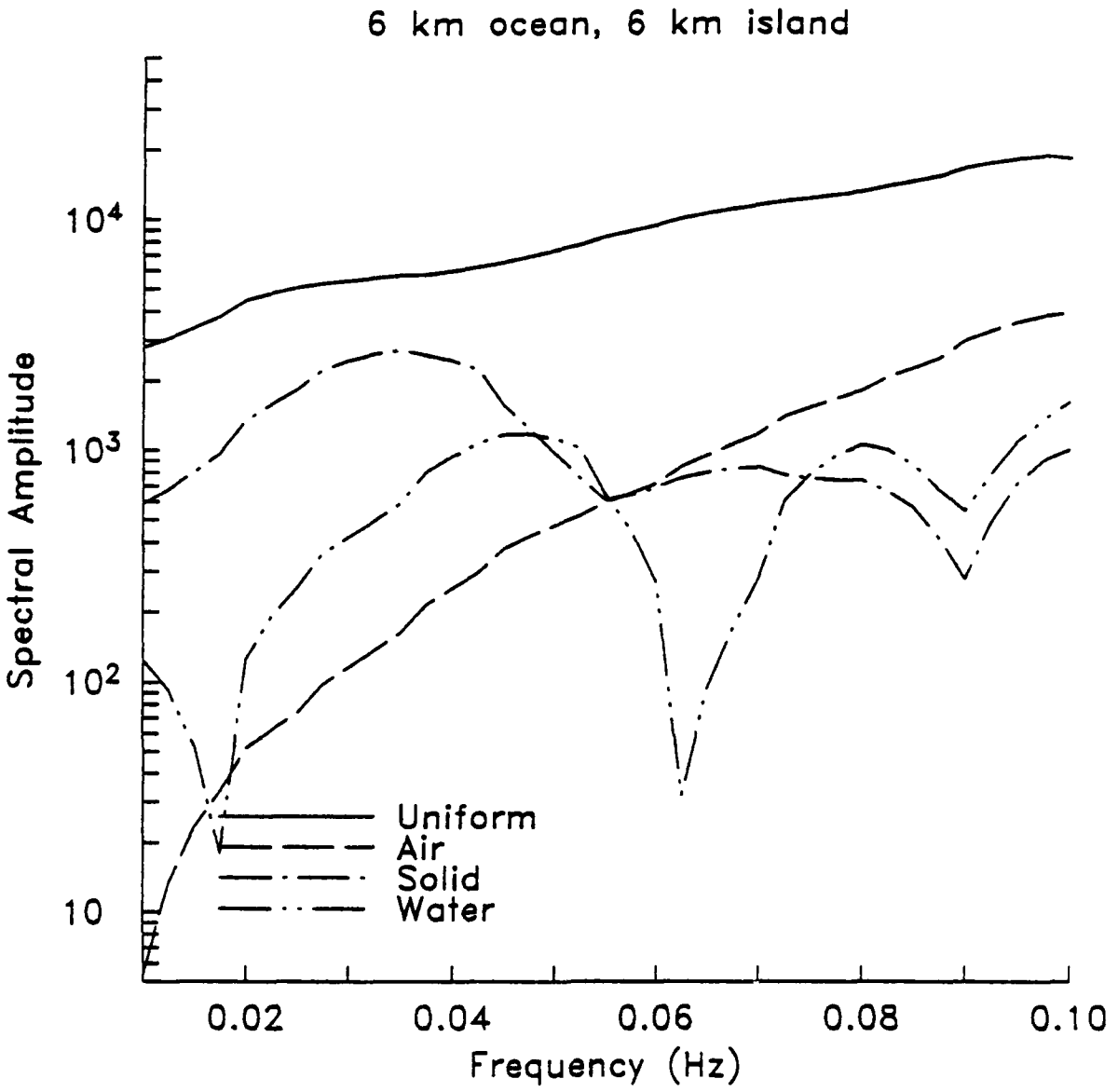

Figure 4. Spectra of surface waves recorded at 390 km from a 6 km radius island across a 6 km deep "ocean" of water, air, and solid. The surface wave amplitudes are sharply reduced at all frequencies in all cases.

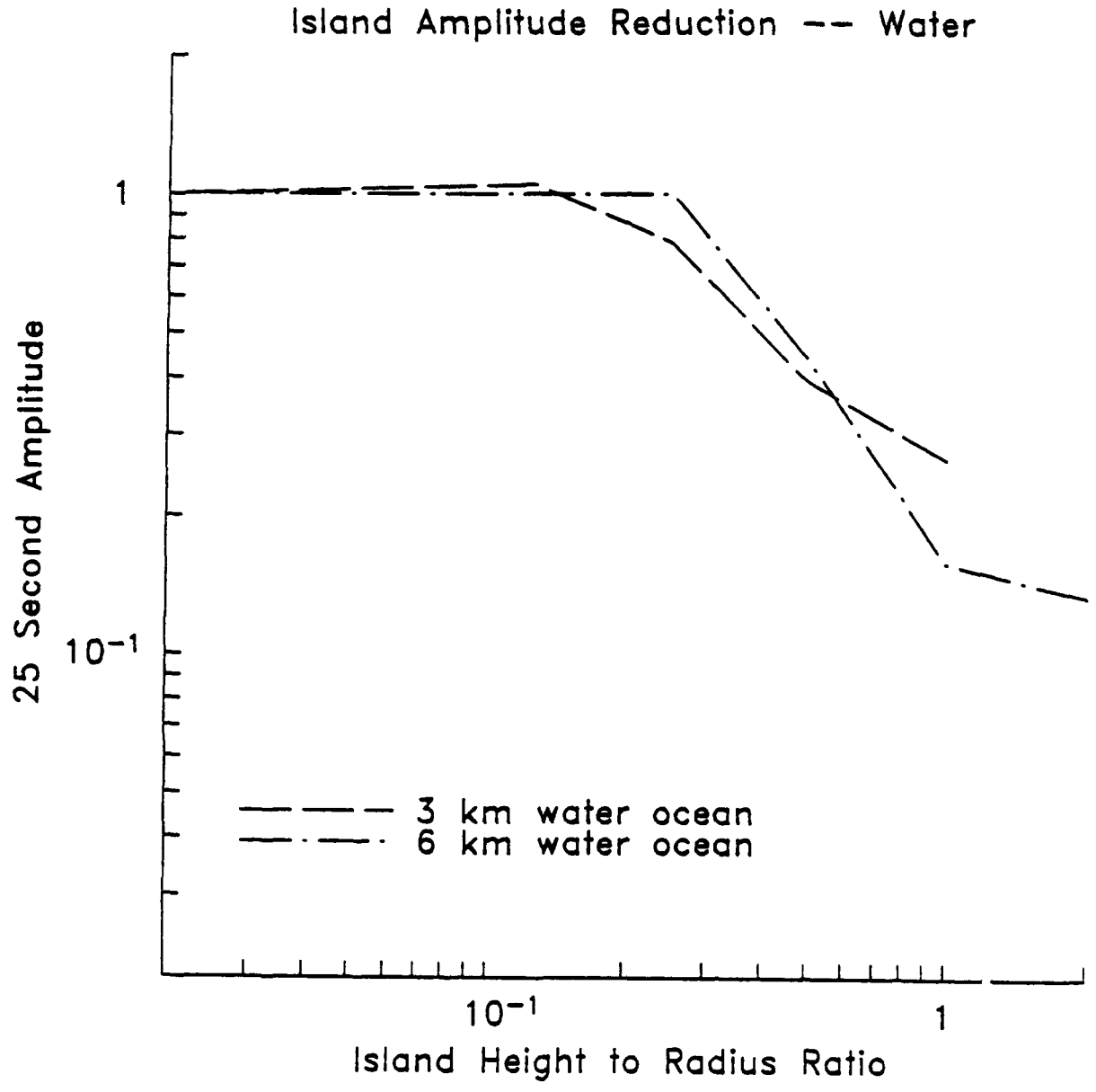

Figure 5. 25 second surface wave amplitude as a function of the island aspect ratio (ratio of island height to radius) for a water ocean.

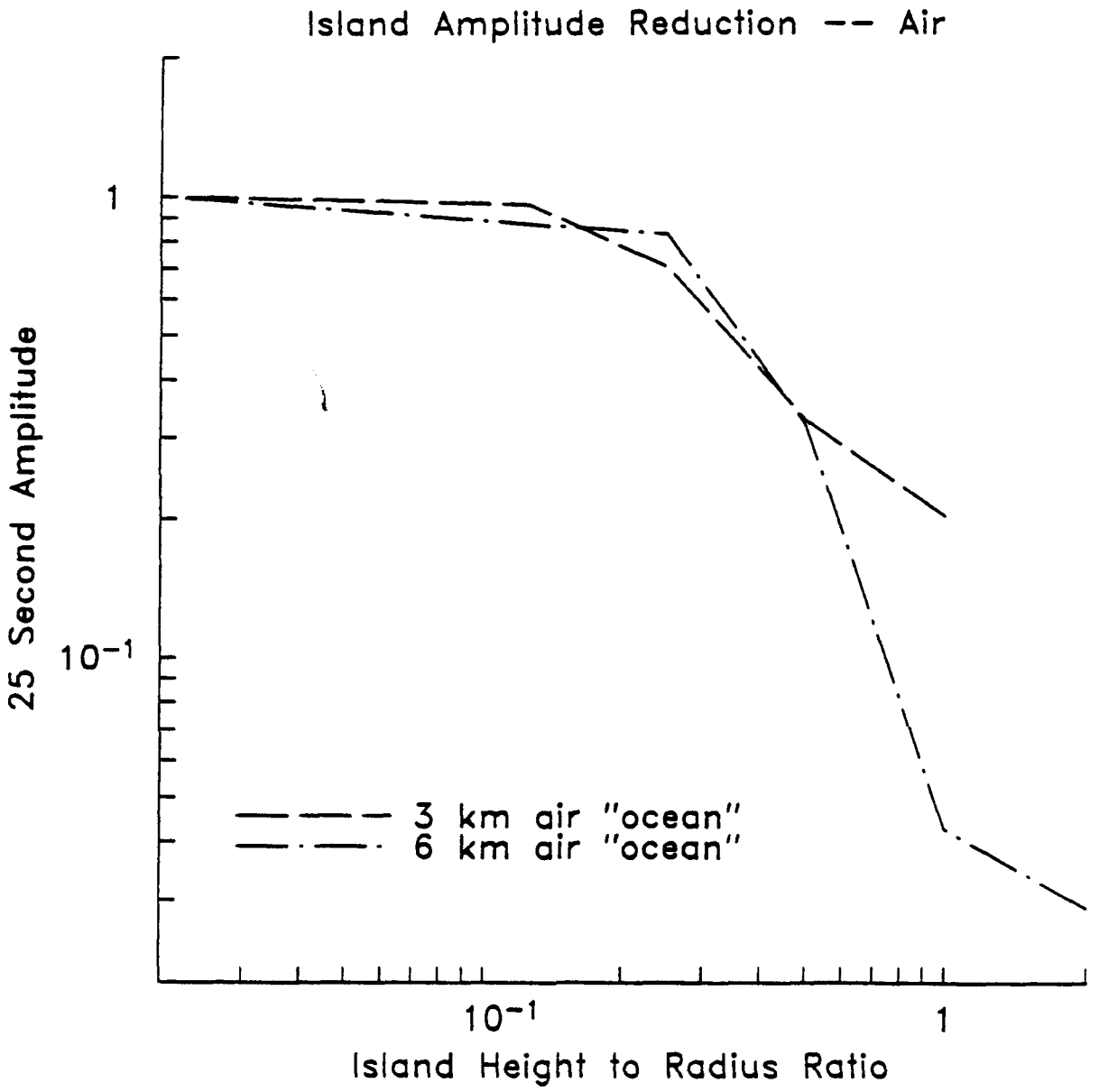

Figure 6. 25 second surface wave amplitude as a function of the aspect ratio for an air-filled "ocean."

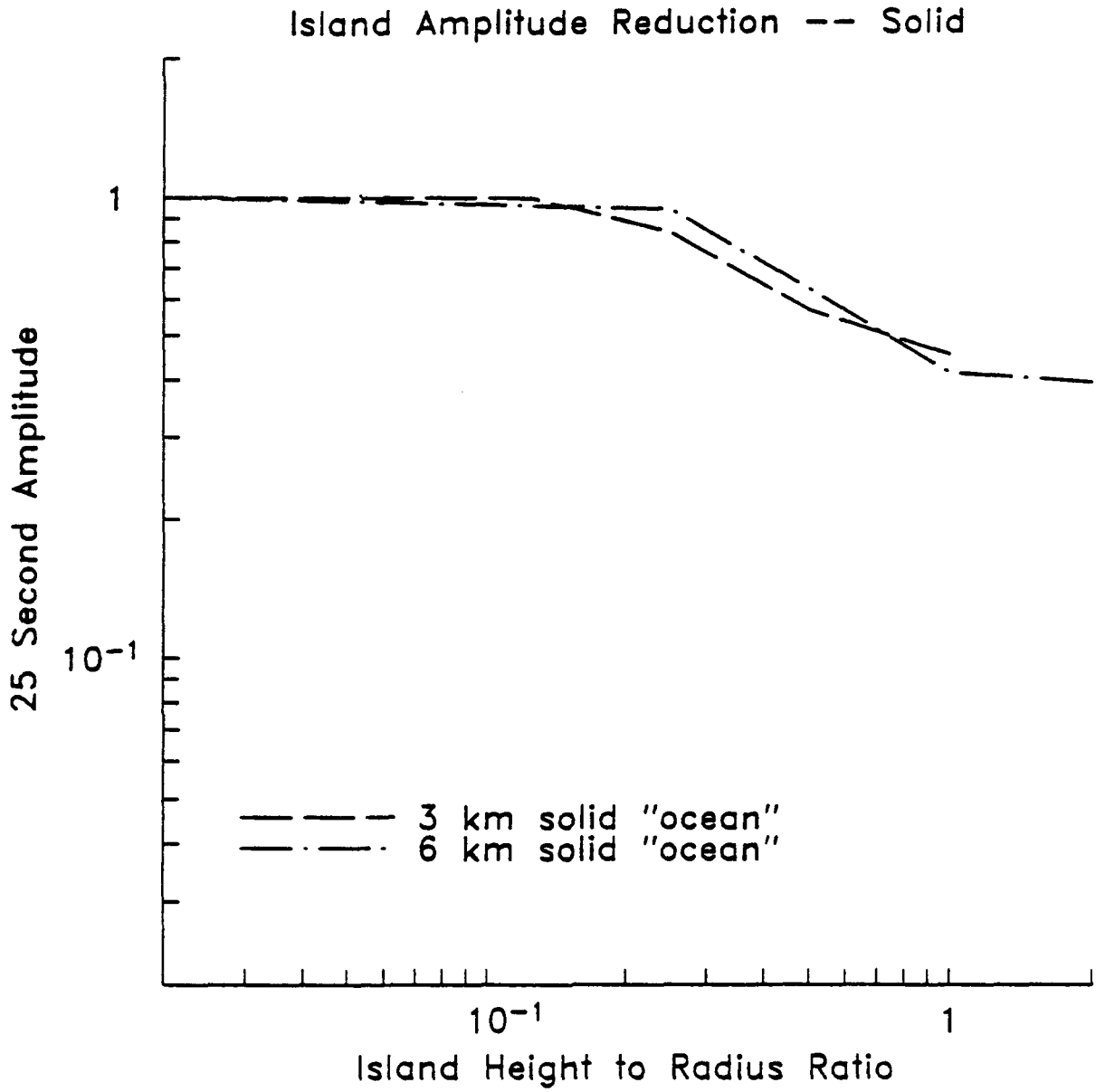

Figure 7. 25 second surface wave amplitude as a function of the aspect ratio for an "ocean" filled with a lower velocity solid.

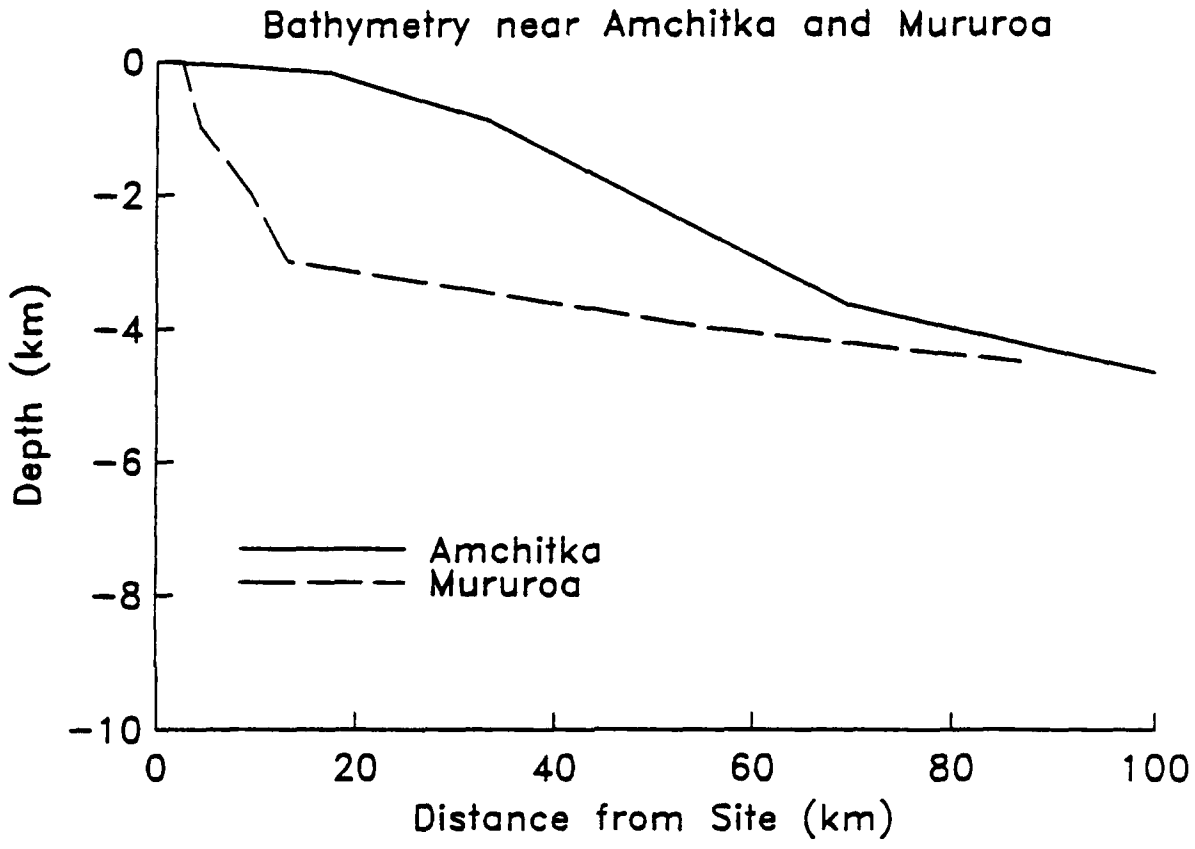

Figure 8. Bathymetry near the Amchitka and Mururoa test sites.

3. SURFACE WAVES FROM AN EXPLOSION IN A MOUNTAIN

Several nuclear test sites are in areas characterized by mountains and steep slopes. Explosions at Novaya Zemlya, Degelen Mountain, and the old French Sahara test site have all been located within and close to mountains. The results of the previous section suggest that this topography could have a strong effect on surface wave generation. An important issue is the effect of depth within and below a mountain on surface wave generation. That is, will the predicted amplitude reduction vanish if the explosion is below the base of the mountain, or will the distortion of the local stress field by the non-planar surface continue to cause an amplitude reduction? The numerical tests described in the previous section used a grid too coarse to answer this question.

In order to examine this effect in more detail, we have performed two numerical experiments. First, we performed a series of plane strain calculations for a Rayleigh wave incident on a mountain, using reciprocity to determine the Rayleigh wave generated by an explosion in the mountain from the dilatation produced by the Rayleigh wave. Second, we performed a calculation for an explosion in a mountain modeled after the actual topography of a mountain at the Novaya Zemlya test site.

3.1. Reciprocity Experiment

The geometry of the plane-strain reciprocal experiment is shown in Figure 9. A planar Rayleigh wave pulse is incident from the left upon a steep mountain with 45 degree slopes and height L = 12 units and radius of 16 (aspect ratio 0.75). The half-space had a compressional velocity of 6 units/sec, and a shear velocity of 3.55 units/sec. Vertical displacements and dilatations are recorded at locations indicated on the figure. Incident displacement and dilatation are then used to normalize each synthetic seismogram to the incident pulse.The seismogram locations correspond to the top, middle, and bottom of the mountain as well as a location deep under the mountain (12 units) and a location on the far side of the mountain (transmitted) at two depths (deep and shallow).

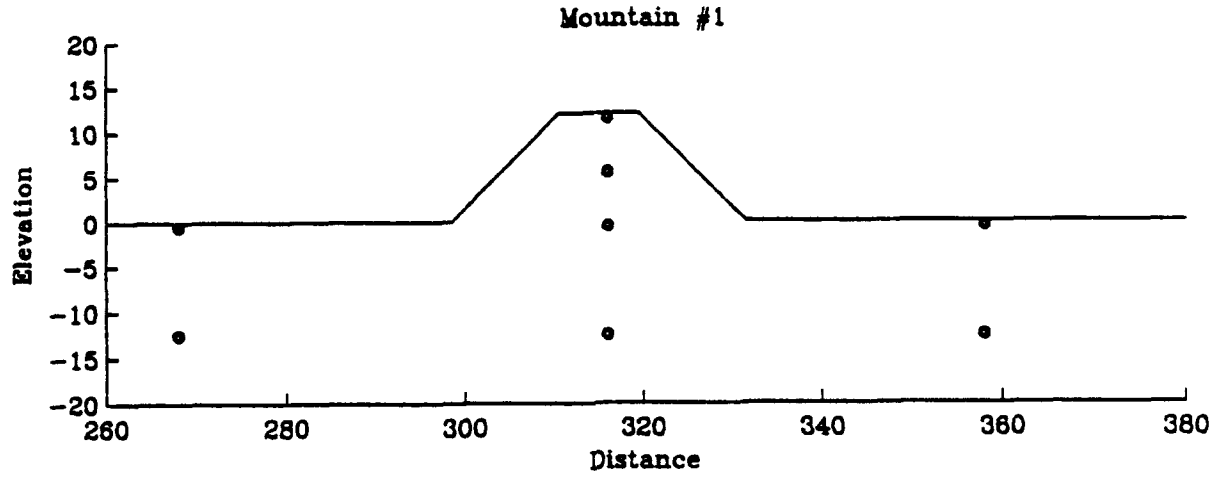

Figure 9. Geometry of the 2-D plane strain reciprocal experiment. The vertical displacements and dilatations due to an incident Rayleigh wave were measured at the locations shown. This is equivalent to measuring the far field Rayleigh wave generated by a vertical point force and explosion, respectively.

By reciprocity the ratio of the recorded displacement to the incident Rayleigh wave vertical displacement is the equivalent to the far-field Rayleigh wave displacement from a vertical point source. Similarly, the ratio of the recorded dilatation to the incident Rayleigh wave is equivalent to the far-field Rayleigh wave from a dilatational (explosion) source. Therefore, we can examine the relative far-field Rayleigh wave excitation from sources within and under the mountain. The effect of transmission through the mountain from source to receiver can be examined as well.

Figure 10 shows the spectral amplitude ratio of the vertical displacements to the incident Rayleigh wave displacement as a function of normalized wavenumber, $k' = \frac{2\pi fL}{c}$, where L = 12 units is the height of the mountain, c = 3.252 units/sec is the Rayleigh wave phase velocity, and f is frequency. This is the reciprocal problem of the Rayleigh wave generated by a point force at the locations shown. We consider $k' << 1$ to be the long period limit while $k' \sim 1$ corresponds to the resonances in the scattering problem. Note that the effect of a vertical point force at the top, middle, bottom, or deep under the mountain is not much different than a source to the side of the mountain with transmission through the mountain. Some amplitude is lost due to scattering but from k'=0.1 to k'=1, the effect is generally less than 30 percent. For k'<1, the effect of the mountain for a vertical point force is comparable to the transmission through the mountain and differs by less than 30 percent.

However, if we examine the problem of explosive sources at these locations, the results are quite different. Figure 11 shows spectral amplitude ratios for dilatational recordings at the respective source locations normalized to the incident Rayleigh wave dilatation. Note that a source deep under the mountain is much the same as a source to the side of the mountain with transmission through the mountain, and for k'=0.1 the effect is less than 30 percent. However, the Rayleigh wave excitation from a source at the top of the mountain is reduced by nearly 90 percent at low frequencies. The deeper the source, under the mountain, the less the effect, but a source located at the bottom of the mountain is still reduced by nearly 50 percent with respect to the half-space source at low frequencies.

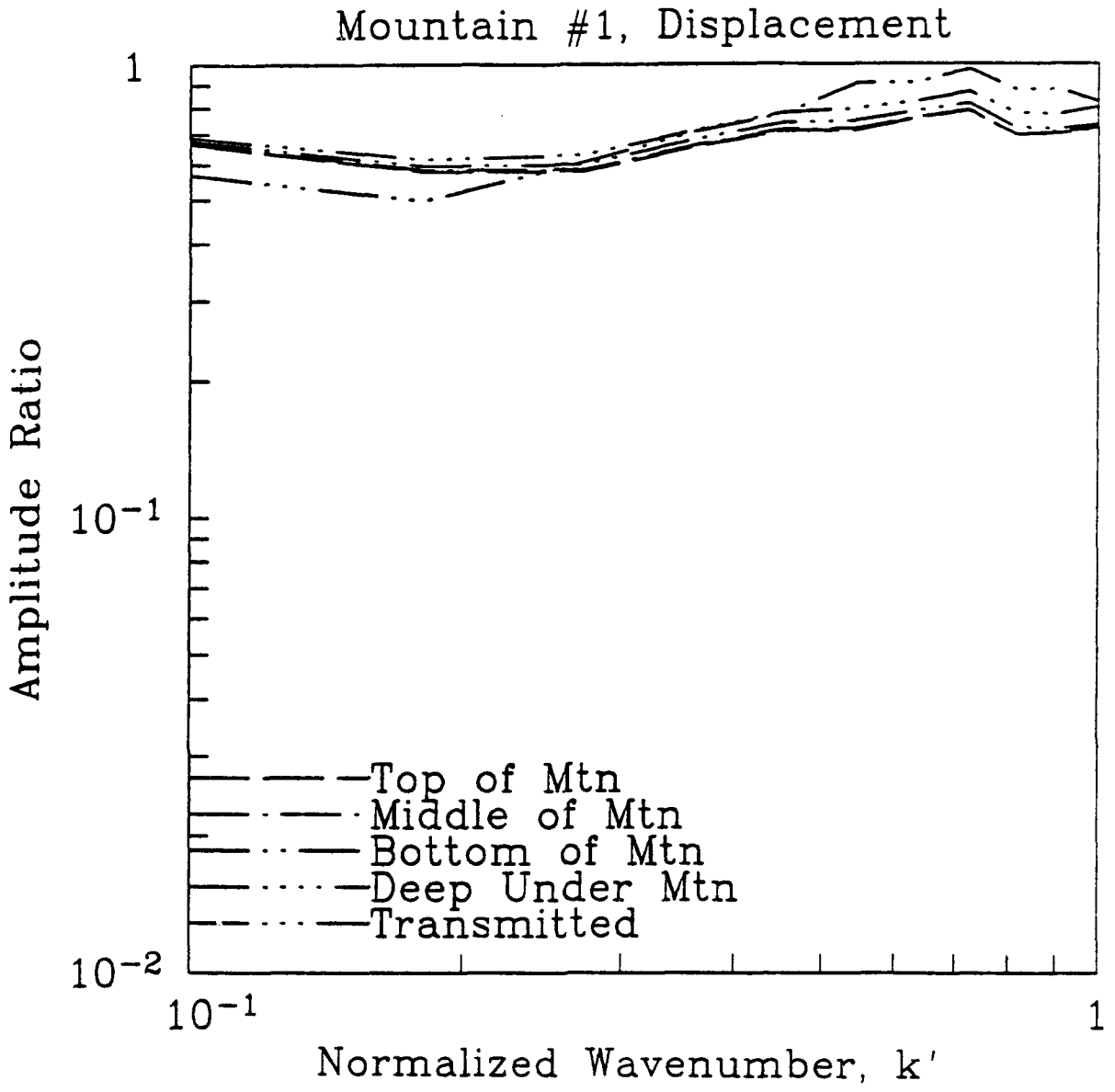

Figure 10. Spectral amplitude ratio of the vertical displacements to the incident Rayleigh wave displacement as a function of normalized wavenumber. This demonstrates that the Rayleigh wave generated by a vertical point force is insensitive to the location of the point force.

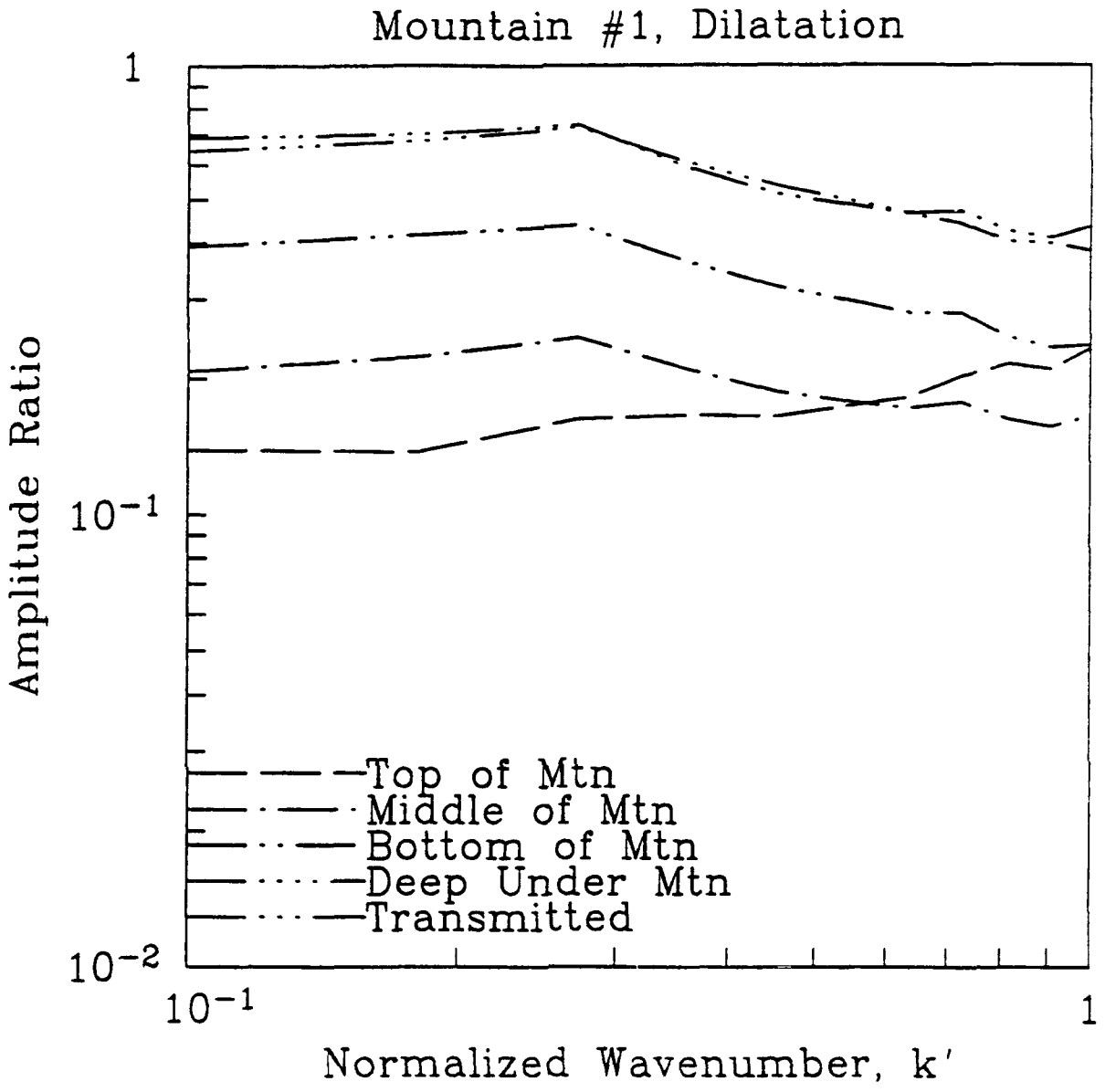

Figure 11. Spectral amplitude ratios for dilatational recordings at the respective source locations normalized to the incident Rayleigh wave dilatation. This demonstrates that the Rayleigh wave amplitude generated by an explosion is quite sensitive to the location of the explosion within the mountain. The Rayleigh wave amplitude is sharply reduced by location in or immediately under a mountain.

This effect has significant implications for long-period Rayleigh wave excitation from underground explosions placed within a mountain. The perturbation of the free surface alters the long-period response of the medium to a dilatational source much more than a vertical force. The reciprocal statement is that the free surface perturbation alters the strain field response much more than the displacement response for an incoming wavefield.

3.2. Novaya Zemlya Mountain Calculation

The rugged topography of the Novaya Zemlya test site is shown in a bedsheet plot based on Defense Mapping Agency (DMA) data in Figure 12. Mountains rise from sea level to over one kilometer in the region where most tests have been located (based on locations from Lilwall and Marshall, 1986). Higher elevations and steeper topography occur outside the region where tests have occurred to date. In Figure 13, we show a SPOT satellite image displayed with the DARPA Yield Estimation System (Murphy, *et al*, 1991) showing the central part of the Novaya Zemlya test site near the Matochkin Shar strait showing the detailed local topography in this region.

A profile was constructed using the actual topography of one of the mountains in the central Novaya Zemlya area. We selected one of the steepest slopes in order to get an estimate of the maximum effect that such topography could have on surface wave generation. This was a profile running to the southeast from the highest peak in the central Matochkin Shar region. The profile was then turned into a finite difference grid with grid elements 100 meters by 100 meters. The surface profile of the finite difference grid is shown in Figure 14.

The grid spacing required by this calculation was too fine to extend to the distances of interest for measuring surface waves. Instead, we saved the displacements and stresses on a monitoring surface outside the source region (below and outside of the elevated region), and used the representation theorem to calculate seismograms at the desired distances. This technique has been described in detail by Bache, *et al.* (1982), Day, *et al.* (1983), and Stevens, *et al.* (1991). The finite difference calculation was performed with uniform material properties throughout the grid (P velocity 6.0 km/sec, S velocity

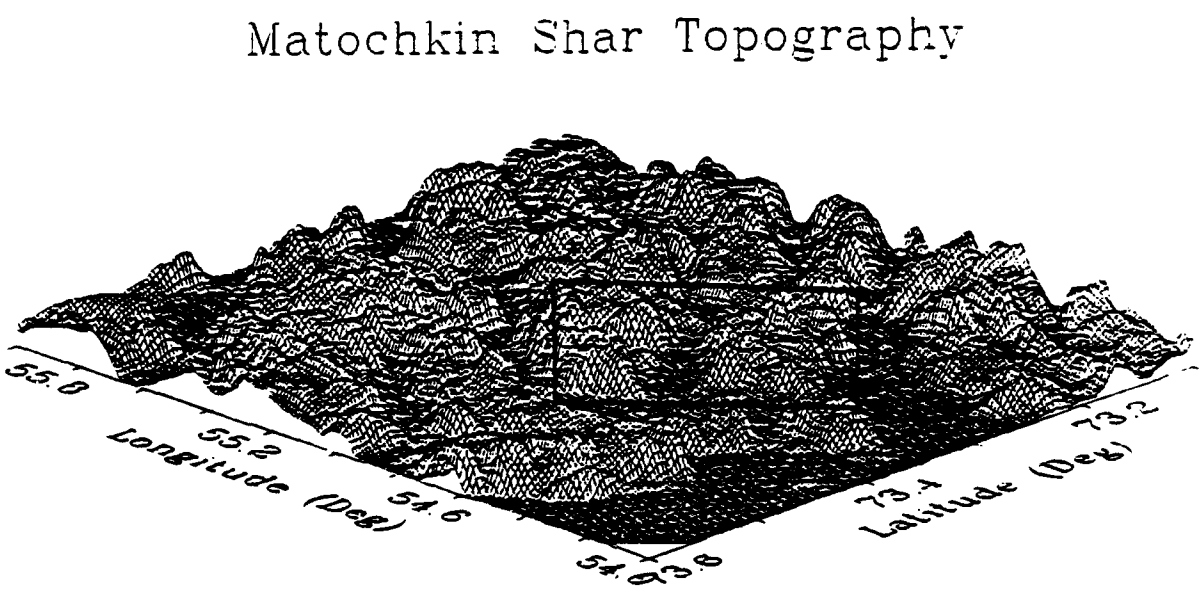

Figure 12. Bedsheet plot showing the topography of the Soviet Novaya Zemlya test site. The rectangle indicates the region where most tests have taken place.

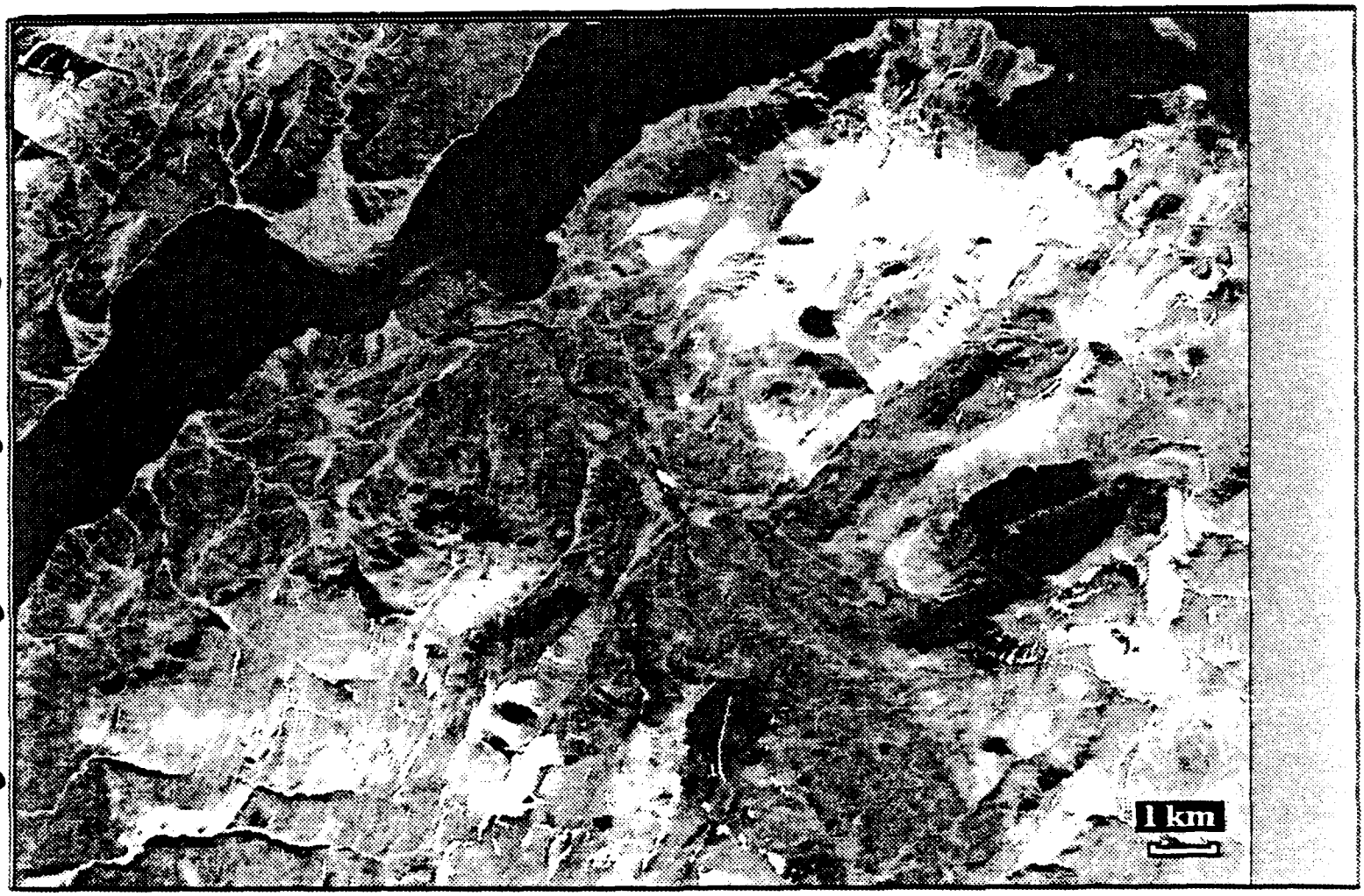

Figure 13. Spot satellite image of the central Novaya Zemlya test site.

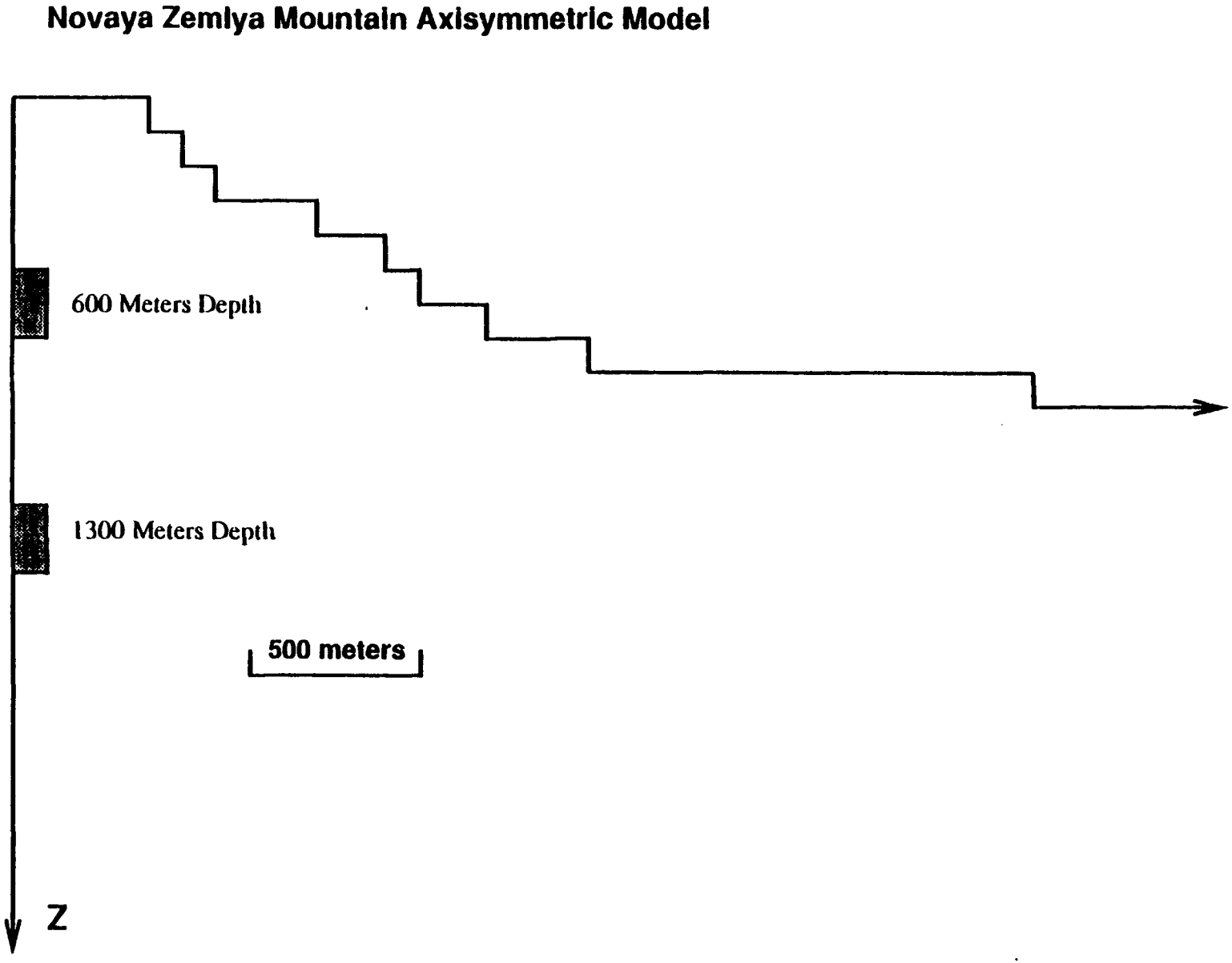

Figure 14. Mountain topography model and explosion source locations used in the finite difference calculations of the Novaya Zemlya mountain.

3.55 km/sec, density 2.50 gm/cm^3). For calculation of the surface wave seismograms, we used the same structure used in the previous set of calculations (see Table 1), but with the upper two kilometers modified to be the same as those used in the finite difference calculation. The source function used in the calculation was the same as in the previous calculations. Calculations were performed for depths of 600 meters and 1300 meters below the top of the mountain as shown in Figure 14. Since the top of the mountain is 1000 meters above sea level, these depths correspond to locations inside the mountain and just below the mountain. Calculations were performed for 15 modes, although the fundamental mode Rayleigh wave dominates in the frequency range of interest.

Synthetic surface wave seismograms were generated from these two finite difference calculations at a distance of 390 km. A synthetic seismogram was also calculated for a point explosion source in the plane layered model without the mountain at a depth of 600 meters. Unlike the mountain simulations, the results of the plane-layered calculation are insensitive to depth for the low frequencies of interest here. The seismograms were phase-match filtered as in the earlier calculations to recover the surface wave spectra. The resulting spectra are shown in Figure 15. The results show that the surface wave amplitude is reduced by almost a factor of three for the explosion within the mountain, and is reduced by a factor of approximately 1.5 for the explosion located just under the mountain compared to the plane-layered surface wave. These results suggest that yield estimates based on surface wave amplitudes for explosions in mountainous regions such as Novaya Zemlya could underestimate the actual explosion yield.

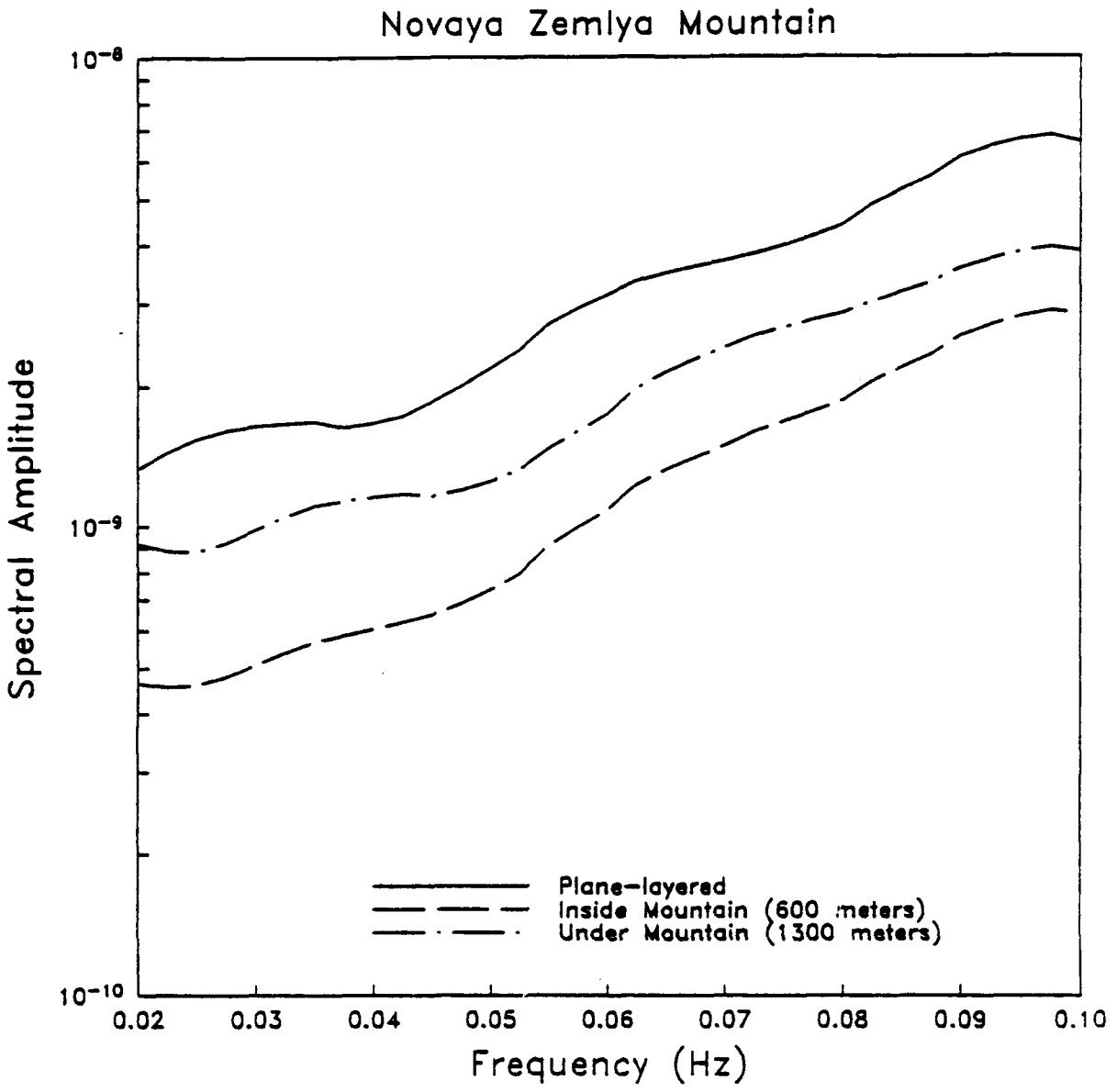

Figure 15. Spectra from the two Novaya Zemlya simulations and an equivalent plane-layered synthetic seismogram.

4. CALCULATION OF AN EXPLOSION IN A SEDIMENTARY VALLEY

The previous sections were concerned with the effect of a near-source boundary or decrease in velocity on surface wave amplitudes. In this section, we examine the converse of this problem: the effect on surface wave amplitudes of a strong increase in velocity in the near-source region.

A 2D axisymmetric linear finite difference calculation was performed to examine the excitation of surface waves from an explosion in a deep low-velocity graben such as Yucca Flats at NTS. As with the Novaya Zemlya calculation, the displacements and tractions were saved on a monitoring surface outside the source region and modal summation methods were used to propagate the seismic waves to a distance of 390 km. This hybrid seismogram is referred to as the representation theorem seismogram. The finite difference calculation was performed with a grid spacing of 125 m and using standard criteria of 10 grids per wavelength the calculation should be good up to 0.5 Hz. The source time function was the same function used in the previous calculations.

The velocity model is shown in Figure 16. The axisymmetric graben has a 10 km diameter and is filled with a 250 m thick layer of low velocity alluvium (α = 1.34 km/s, β = 0.603 km/s, ρ = 1.70 g/cm^3 where α represents P velocity, β shear velocity, and ρ density), a 250 m thick layer of unsaturated tuff (α = 2.14 km/s, β = 0.963 km/s, ρ = 1.90 g/cm^3), and a 500 m thick layer of saturated tuff (α = 3.00 km/s, β = 1.50 km/s, ρ = 2.00 g/cm^3), The basement is paleozoic carbonates (α = 5.00 km/s, β = 3.00 km/s, ρ = 2.70 g/cm^3), with a surface weathered layer 500 m thick outside of the graben (α = 4.50 km/s, β = 2.25 km/s, ρ = 2.50 g/cm^3). This model is based on models used by McLaughlin, *et al.* (1987) and Ferguson (1981).

For the purposes of propagating waves outside the graben to a distance of 390 km, model BR3 (Table 2) was used. This is a modified version of the basin and range model BR2 of McLaughlin, *et al.* (1988). Plane layered synthetics were computed for comparison with the representation theorem seismogram. The plane layered synthetics were propagated in the BR3 model

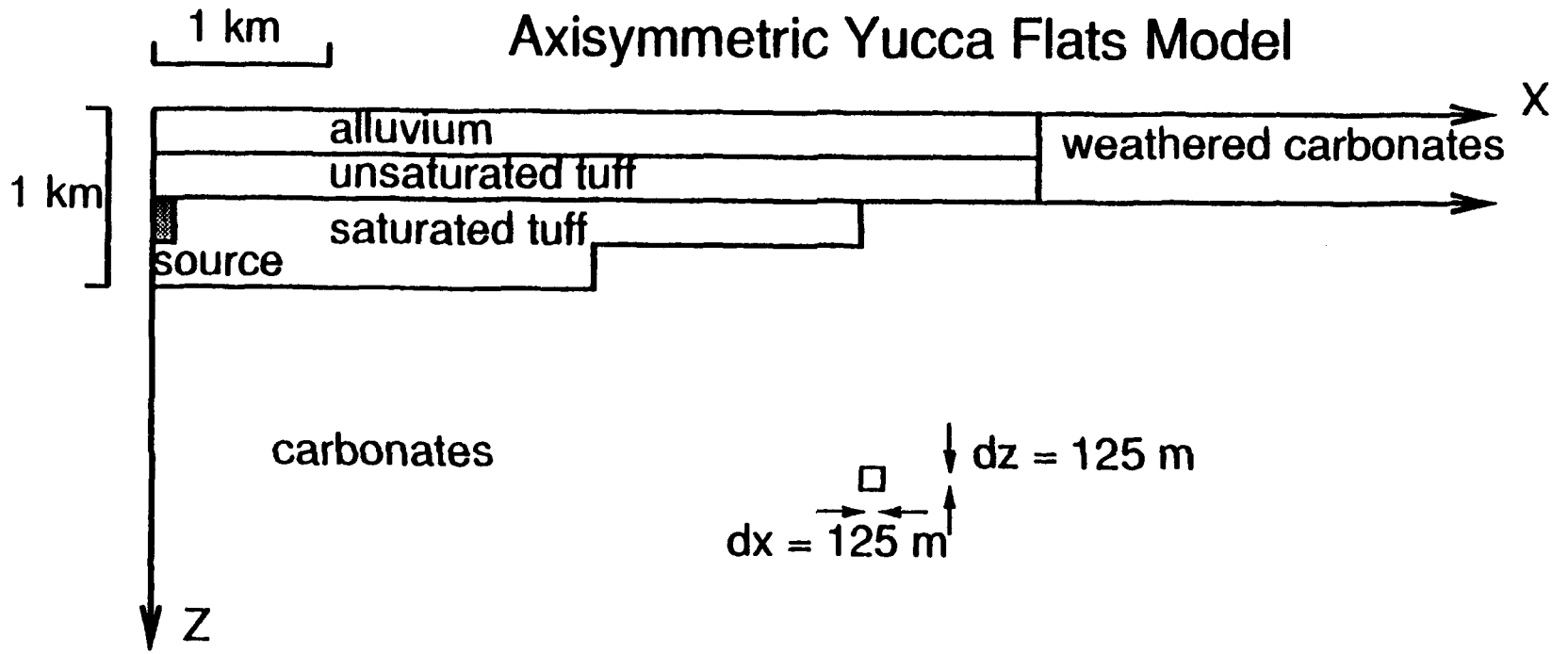

Figure 16. Model used for axisymmetric Yucca Flats simulation.

Table 2
Basin and Range Model BR3

Depth km	Thickness km	P-Velocity km/sec	S-Velocity km/sec	Density gm/cc	Q
0.5	0.5	4.50	2.25	2.50	50.
2.0	1.5	5.00	3.00	2.70	100.
3.5	1.5	5.80	3.40	2.80	125.
6.5	3.0	6.00	3.46	2.90	125.
20.5	14.0	6.30	3.64	2.90	150.
24.5	4.0	6.50	3.75	2.90	150.
28.5	4.0	6.80	3.93	3.00	150.
34.5	6.0	6.90	3.98	3.00	150.
38.5	4.0	7.80	4.50	3.20	200.
42.5	4.0	7.84	4.50	3.20	200.
46.5	4.0	7.88	4.50	3.20	200.
50.5	4.0	7.92	4.50	3.20	200.
54.5	4.0	7.96	4.50	3.20	200.
56.5	2.0	8.00	4.50	3.20	200.
60.5	4.0	8.05	4.50	3.20	200.
70.5	10.0	7.90	4.40	3.20	75.
80.5	10.0	7.80	4.20	3.20	75.
100.5	20.0	7.80	4.20	3.20	75.
120.5	20.0	7.90	4.50	3.20	75.
180.5	60.0	8.00	4.55	3.30	75.
∞	∞	8.10	4.60	3.40	150.

for explosion sources in the BR3 model and in the Yucca model, where the Yucca model was identical to the BR3 model below 2 km depth, with properties given by a vertical line through the explosion source in the Yucca Valley model in the upper 2 km (Table 3). In each case the source was a point explosion with the same reduced displacement potential (ψ_∞, not moment) as the representation theorem seismogram. Propagation from the source structure to the path structure was accomplished using a transmission coefficient based on conservation of energy (Bache, *et al*, 1978; Stevens, 1986a). The synthetic seismograms were convolved with the same source function used in the representation theorem seismogram. Twenty-seven modes were computed, and used in both the representation theorem and the plane-layered

Table 3
Yucca Valley Model

Depth km	Thickness km	P-Velocity km/sec	S-Velocity km/sec	Density gm/cc
0.25	0.25	1.340	0.603	1.70
0.50	0.25	2.140	0.963	1.90
1.00	0.50	3.000	1.500	2.00
2.00	1.00	5.000	3.000	2.70

seismograms, although only the first few modes have significant amplitude in the seismograms, and the fundamental mode dominates at frequencies less than 0.1 Hz.

The seismograms are shown in Figure 17. There is a significant increase in amplitude of the representation theorem seismogram relative to the Yucca/BR3 seismogram. The spectra of the three seismograms are shown in Figure 18. The spectrum of the representation theorem seismogram is approximately twice the amplitude of the Yucca/BR3 seismogram. In fact, the amplitude is intermediate between the spectrum of the Yucca/BR3 seismogram and the BR3/BR3 seismogram, in spite of the fact that the BR3/BR3 seismogram had a moment four times as large as in the representation theorem calculation.

Previously, Vassiliou, *et al.* (1987) investigated Rayleigh wave propagation in a 3D ultrasonic scale model of the Yucca Flats graben. Ultrasonic scale modeling has the advantage that 3D models can be constructed and experiments performed that would be computationally impractical. They concluded that there was no significant long period enhancement of surface waves from sources in a graben structure filled with low velocity material. They used a vertical point force as a source in the high velocity medium outside the graben structure and measured vertical displacement at locations in the Yucca Flats model. However, this was an incorrect use of the elastodynamic reciprocity theorem, which requires the experimenters to measure dilational strain at locations in the Yucca Flats model

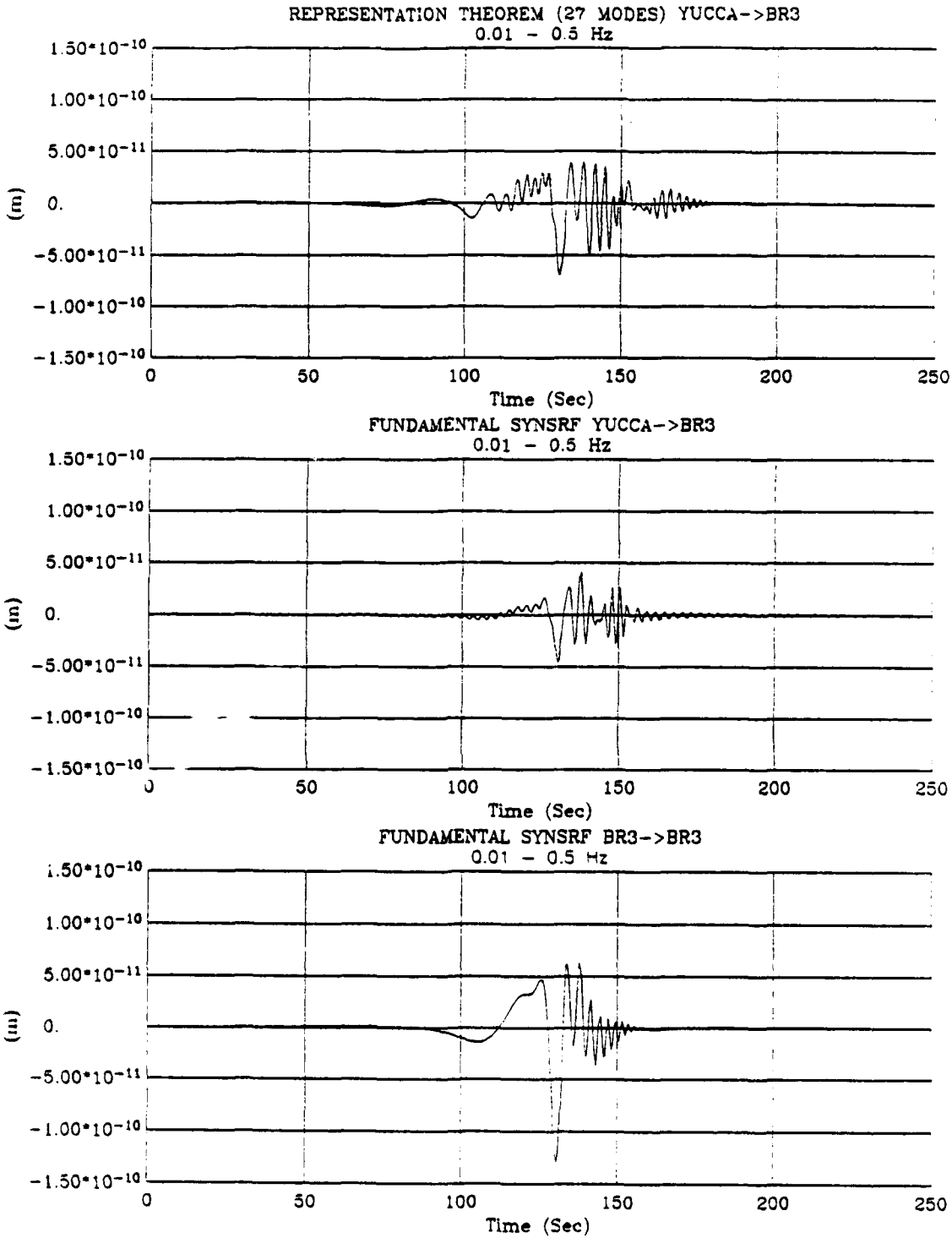

Figure 17. Seismogram from the Yucca Flats simulation (top) together with plane-layered seismograms for a source with the same RDP in the BR3 model (bottom), and in the Yucca model transmitted into the BR3 model (middle).

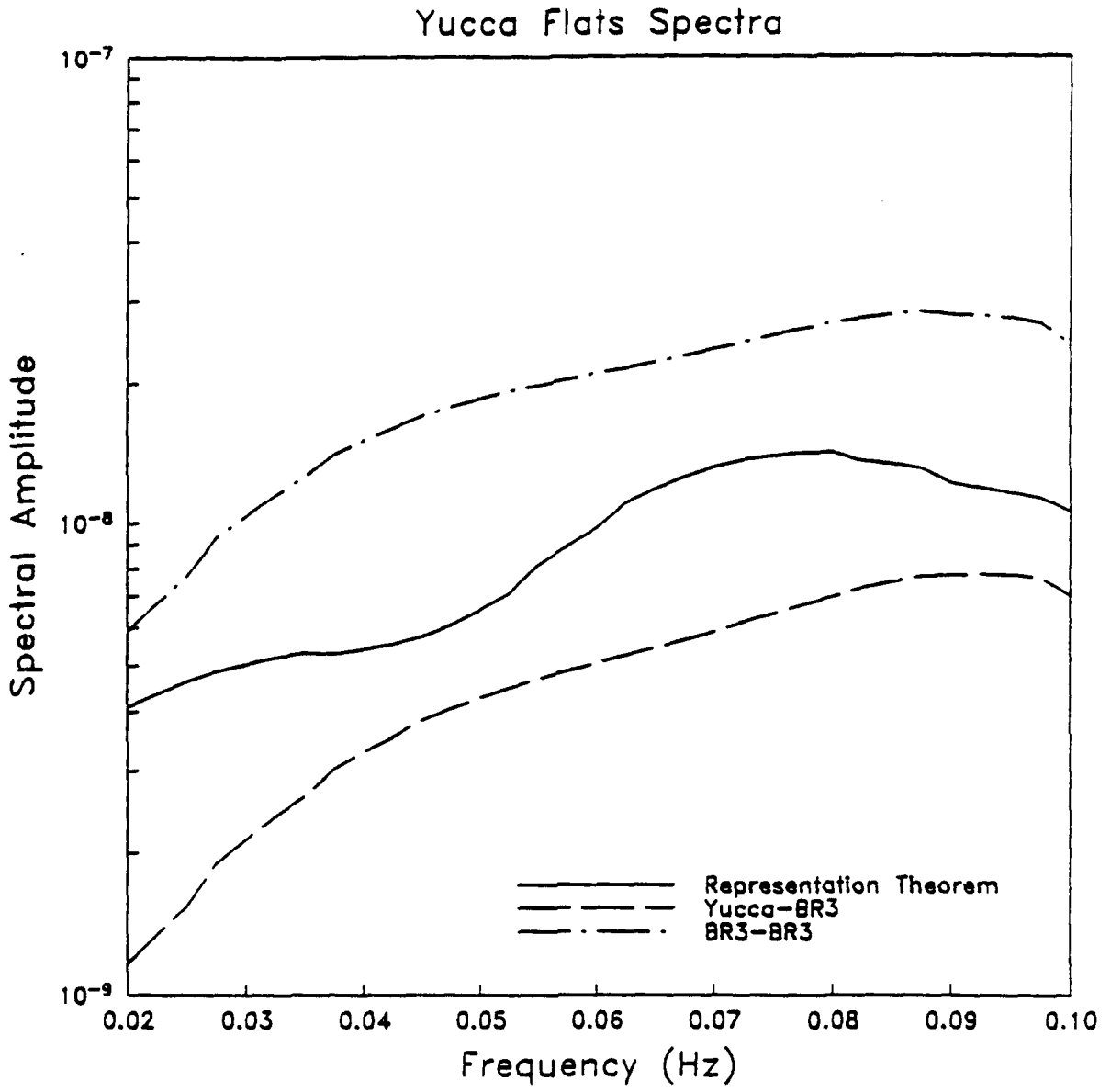

Figure 18. Spectra from the Yucca Flats simulation and the two plane-layered synthetic seismograms.

rather than vertical displacement. Consequently, they could only conclude that vertical point force sources would not exhibit long period enhancement of surface wave excitation. Due to the difficulty of measuring dilatational strain and/or using explosion sources in the physical scale models, it is not possible to truly model the surface wave excitation from explosions in the 3D model.

Our computational modeling has shown that strain is more sensitive to lateral heterogeneity and free surface topography than displacement. Consequently seismic excitation from a moment tensor source is more sensitive to near-source heterogeneity than a source composed of simple point forces.

5. CONCLUSIONS

We have completed a series of finite difference simulations designed to model the effect of an island/ocean interface, mountain/air boundary or near-source material property change on surface wave amplitudes. The results strongly suggest that explosion yield estimates based on surface waves may be substantially affected by variations in near source material properties, and in particular by near source boundaries. The effect of a free surface or ocean/island interface close to the source can substantially reduce surface wave amplitudes. This effect could be substantial for an explosion in a salt dome surrounded by sediments, for example. A reduction in material properties outside, but close to, the source region can also reduce surface wave amplitudes to a lesser extent. Furthermore, an increase in material properties near the source region can cause amplification of the explosion-generated surface waves.

These results are clearly important for seismic yield estimation, and may also explain some anomalies that have been observed at certain test sites. Some Novaya Zemlya explosions, for example, are reduced in amplitude at low frequencies and phase shifted (Stevens and McLaughlin, 1988; Tucker, *et al.*, 1989). Similarly, it has been suggested that surface wave amplitudes are higher (for the same yield) for explosions in the southern part of Yucca Valley than for explosions in the northern part. Finally, although we have concentrated on the effect of material boundaries on long period surface waves, similar effects may exist for regional surface waves, particularly for Rg generated by quarry blasts.

In this study, we have concentrated on problems with simple or representative geometries in order to try to quantify the general effects to be expected from the presence of material boundaries near explosions on long period surface waves under typical conditions. The same procedure could be used, however, to explicitly model specific explosions or regions of interest for problem events that occur with complex geometries. The same procedures can also be applied to calculations of regional surface waves at higher frequencies.

6. ACKNOWLEDGEMENTS

The 2D finite difference calculations conducted on the Phillips Laboratory CRAY-2 were made possible by Mr. J. Lewkowicz and Ms. J. McPhetres of Phillips Laboratory LWH. This work was monitored by AFTAC under contract F08606-89-C-0022.

7. REFERENCES

Bache, T. C., W. L. Rodi, and D. G. Harkrider (1978), "Crustal Structures Inferred from Rayleigh Wave Signatures of NTS Explosions, *Bull. Seism. Soc. Am., 68, pp. 1399-1413.*

Bache, T. C., S. M. Day and H. J. Swanger (1982), "Rayleigh Wave Synthetic Seismograms from Multi-Dimensional Simulations of Underground Explosions", *Bull. Seism. Soc. Am., 72, pp. 15-28.*

Day, S. M., N. Rimer and J. T. Cherry (1983), "Surface Waves from Underground Explosions With Spall: Analysis of Elastic and Nonlinear Source Models," *Bull. Seism. Soc. Am., 73, pp. 247-264.*

DMA (1983), "Omega, South Pacific Ocean, Isles Tuamotu (Eastern Part): HAO to FANGATAUFA," Defense Mapping Agency map number 83024.

Ferguson, J. F. (1981). Geophysical Investigations of Yucca Flat, Nevada, PhD Thesis, Southern Methodist University, Dallas, Texas, 102 pp.

Lilwall, R. C., and P. D. Marshall (1986), "Body Wave Magnitudes and Locations of Soviet Underground Explosions at the Novaya Zemlya Test Site," Atomic Weapons Research Establishment Report O17/86.

McLaughlin, K. L., L. M. Anderson, and A. C. Lees (1987). Effects of Local Geologic Structure on Yucca Flats, Nevada Test Site, Explosion Waveforms: Two-Dimensional Linear Finite Difference Simulations, *Bull. Seism. Soc. Am., 77, 1211-1222.*

McLaughlin, K. L., T. G. Barker, S. M. Day, B. Shkoller, and J. L. Stevens (1988), "Effects of Depth of Burial and Tectonic Strain Release on Regional and Teleseismic Explosion Waveforms," S-CUBED Scientific Report No. 2 submitted to Air Force Geophysics Laboratory, AFGL-TR-88-0314, SSS-R-88-9844, November.

McLaughlin, K. L., T. G. Barker, S. M. Day, B. Shkoller and J. L. Stevens (1991), "Effects of Subduction Zone Structure on the Propagation of Explosion-Generated Long-Period Rayleigh Waves," S-CUBED Technical Report submitted to AFTAC, SSS-TR-91-12132.

Murphy, J. R., J. L. Stevens, D. C. O'Neill, B. W. Barker, K. L. McLaughlin, and M. E. Marshall (1991), "Development of a Comprehensive Seismic Yield Estimation System for Underground Nuclear Explosions," S-CUBED Scientific Report No. 2 submitted to Phillips Laboratory, PL-TR-91-2161, SSS-TR-91-12434, May.

Olsen, K. H., J. N. Stewart, J. E. McNeil and M. J. Vitousek (1972), "Long-Period Water-Wave Measurements for the Milrow and Cannikin Nuclear Explosion," *Bull. Seism. Soc. Am., V. 62, 1559-1578.*

Stevens, J. L. (1986a), "Estimation of Scalar Moments from Explosion-Generated Surface Waves, *Bull. Seism. Soc. Am., 76, 123-151.*

Stevens, J. L. (1986b), "Analysis of Explosion-Generated Rayleigh and Love Waves from East Kazakh, Amchitka and Nevada Test Sites, " AFGL-TR-86-0043.

Stevens, J. L., and K. L. McLaughlin (1988), "Analysis of Surface Waves from the Novaya Zemlya, Mururoa, and Amchitka Test Sites, and Maximum Likelihood Estimation of Scalar Moments from Earthquakes and Explosions," S-CUBED Technical Report submitted to Air Force Technical Applications Center, SSS-TR-89-9953, September.

Stevens, J. L., T. G. Barker, S. M. Day, K. L. McLaughlin and B. Shkoller (1991). Two and Three Dimensional Numerical Modeling of Surface Waves from Underground Explosions, Analysis of Data from Soviet JVE, and Magnitude/Yield Relations from East Kazakh Explosions, S-CUBED Technical Report submitted to Air Force Technical Applications Center, SSS-TR-91-12241, February.

Stevens, J. L., T. G. Barker, S. M. Day, K. L. McLaughlin, N. Rimer, and B. Shkoller (1991), "Simulation of Teleseismic Body Waves, Regional Seismograms, and Rayleigh Wave Phase Shifts Using Two-Dimensional Nonlinear Models of Explosion Sources," AGU Monograph on Explosion Source Phenomenology, S. Taylor, Editor, in press.

Toksoz, M. N. and H. H. Kehrer (1972), "Tectonic Strain Release Characteristics of CANNIKIN," *Bull. Seism. Soc. Am., 62, 1425-1438.*

Tucker, W. C., G. R. Mellman and J. W. Given (1989), "Using Long Period Surface Waves to Estimate the Isotropic Moment of Underground Explosions at Novaya Zemlya," Sierra Geophysics Report SGI-R-89-141.

Vassiliou, M. S., M. Abdel-Gawad, and B. R. Tittmann (1987). Ultrasonic Physical Modeling of Seismic Wave Propagation from Graben-Like Structures, AFGL-TR-87-0256, Rockwell International Science Center, Thousand Oaks, CA 91360.

von Seggern, D. (1978), "Intersite Magnitude-Yield Bias Exemplified by the Underground Nuclear Explosions MILROW, BOXCAR and HANDLEY," Teledyne Geotech Report SDAC-TR-77-4.

DISTRIBUTION LIST
FOR UNCLASSIFIED REPORTS
DARPA-FUNDED PROJECTS
(Last Revised: 24 Feb 92)

RECIPIENT	NUMBER OF COPIES
DEPARTMENT OF DEFENSE	
DARPA/NMRO ATTN: Dr R. Alewine 3701 N. Fairfax Drive Arlington VA 22203-1714	1
Defense Intelligence Agency Directorate for Scientific and Technical Intelligence Washington DC 20340-6160	1
Defense Nuclear Agency Shock Physics Directorate/SD Washington DC 20305-1000	1
Defense Technical Information Center Cameron Station Alexandria VA 22314	2
DEPARTMENT OF THE AIR FORCE	
AFOSR/NP Bldg 410, Room C222 Bolling AFB Washington DC 20332-6448	1
AFTAC/STINFO Patrick AFB FL 32925-6001	1
AFTAC/TT Patrick AFB FL 32925-6001	3
AFWL/NTESG Kirtland AFB NM 87117-6008	1
PL/GPEH ATTN: Mr James Lewkowicz Earth Sciences Division Hanscom AFB MA 01731-5000	1

DEPARTMENT OF THE NAVY

NORDA 1
ATTN: Dr J.A. Ballard
Code 543
NSTL Station MS 39529

DEPARTMENT OF ENERGY

Department of Energy 1
ATTN: Mr Max A. Koontz (DP-5.1, 4B041)
PO Box 23865
Washington DC 20024

Lawrence Livermore National Laboratory 3
ATTN: Dr J. Hannon, Dr S. Taylor, and Dr K. Nakanishi
University of California
PO Box 808
Livermore CA 94550

Los Alamos Scientific Laboratory 2
ATTN: Dr C. Newton
PO Box 1663
Los Alamos NM 87544

Sandia National Laboratories 1
ATTN: Mr P. Stokes, Dept 9110
PO Box 5800
Albuquerque NM 87185

OTHER GOVERNMENT AGENCIES

Central Intelligence Agency 1
ATTN: Dr L. Turnbull
OSI/NED, Room 5P0130
Washington DC 20505

US Arms Control and Disarmament Agency 1
ATTN: Dr M. Eimer
Verification and Intelligence Bureau, Rm 5741
Washington DC 20451

US Arms Control and Disarmament Agency 1
ATTN: Mr R.J. Morrow
320 21st Street NW
Washington DC 20451

US Geological Survey 1
ATTN: Dr T. Hanks
National Earthquake Research Center
345 Middlefield Road
Menlo Park CA 94025

OTHER GOVERNMENT AGENCIES (continued)

US Geological Survey MS-913 — 1
ATTN: Dr R. Masse
Global Seismology Branch
Box 25046, Stop 967
Denver Federal Center
Denver CO 80225

UNIVERSITIES

Boston College — 1
ATTN: Dr A. Kafka
Western Observatory
381 Concord Road
Weston MA 02193

California Institute of Technology — 1
ATTN: Dr D. Harkrider
Division of Geological and Planetary Sciences
Seismological Laboratory
Pasadena CA 91125

Columbia University — 1
ATTN: Dr L. Sykes
Lamont-Doherty Geological Observatory
Palisades NY 10964

Cornell University — 1
ATTN: Dr M. Barazangi
INSTOC
3126 Snee Hall
Ithaca NY 14853

Harvard University — 1
ATTN: Dr J. Woodhouse
Hoffman Laboratory
20 Oxford Street
Cambridge MA 02138

Massachusetts Institute of Technology — 3
ATTN: Dr S. Soloman, Dr N. Toksoz, and Dr T. Jordan
Earth Resources Laboratory
42 Carleton Street, E34-440
Cambridge MA 02142

Southern Methodist University — 2
ATTN: Dr E. Herrin and Dr B. Stump
Geophysical Laboratory
Dallas TX 75275

UNIVERSITIES (continued)

State University of New York at Binghamton 1
ATTN: Dr F. Wu
Department of Geological Sciences
Binghamton NY 13902-6000

St Louis University 2
ATTN: Dr B. Mitchell and Dr R. Herrmann
Department of Earth and Atmospheric Sciences
3507 Laclede
St. Louis MO 63156

Pennsylvania State University, The 1
ATTN: Dr S. Alexander
Geosciences Department
537 Deike Building
University Park PA 16802

University of Arizona 1
ATTN: Dr T. Wallace
Department of Geosciences, Bldg 77
Tucson AZ 85721

University of California, Berkeley 1
ATTN: Dr T. McEvilly
Department of Geology and Geophysics
Berkeley CA 94720

University of California, Los Angeles 1
ATTN: Dr L. Knopoff
405 Hilgard Avenue
Los Angeles CA 90024

University of California, San Diego 1
ATTN: Dr J. Orcutt
Scripps Institute of Oceanography, IGPP, A-025
La Jolla CA 92093

University of California, Santa Cruz 1
ATTN: Dr T. Lay
Earth Sciences Board, Institute of Tectonics
Santa Cruz CA 95064

University of Colorado 1
ATTN: Dr C. Archambeau
CIRES, Campus Box 449
Boulder CO 80309

University of Illinois 1
ATTN: Dr S. Grand
Department of Geology
1301 West Green Street
Urbana IL 61801

UNIVERSITIES (continued)

University of Southern California 1
ATTN: Dr K. Aki
Center for Earth Sciences
University Park
Los Angeles CA 90089-0741

DEPARTMENT OF DEFENSE CONTRACTORS

Analytical Sciences Corporation, The 1
ATTN: Document Control (Dr Richard Sailor)
55 Walkers Brook Drive
Reading MA 01867

Applied Theory, Inc. 1
ATTN: Dr J. Trulio
930 South La Brea Avenue, Suite 2
Los Angeles CA 90036

Center for Seismic Studies 2
ATTN: AFTAC Representative
1300 N. 17th Street, Suite 1450
Arlington VA 22209

ENSCO, Inc. 1
ATTN: Mr John R. Stevenson
PO Box 1346
Springfield VA 22151

ENSCO, Inc. 1
ATTN: Dr R. Kemerait
445 Pineda Court
Melbourne FL 32940-7508

Gould, Inc. 1
ATTN: Mr R.J. Woodard
Chesapeake Instrument Division
6711 Baymeado Drive
Glen Burnie MD 21061

Maxwell Laboratories, Inc. 1
S-CUBED Reston Geophysics Office
Reston International Center
ATTN: Mr J. Murphy, Suite 1212
11800 Sunrise Valley Drive
Reston VA 22091

Pacific Sierra Research Corp. 1
ATTN: Mr F. Thomas
12340 Santa Monica Boulevard
Los Angeles CA 90025

DEPARTMENT OF DEFENSE CONTRACTORS (Continued)

Rockwell International 1
ATTN: B. Tittmann
1049 Camino Dos Rios
Thousand Oaks CA 91360

Rondout Associates, Inc. 1
ATTN: Dr P. Pomeroy
PO Box 224
Stone Ridge NY 12484

Science Applications International Corporation 1
ATTN: Document Control (Dr T. Bache, Jr.)
10210 Campus Point Drive
San Diego CA 92121

Science Horizons 2
ATTN: Dr T. Cherry and Dr J. Minster
710 Encinitas Blvd, Suite 101
Encinitas CA 92024

S-CUBED, A Division of Maxwell 1
Laboratories, Inc
ATTN: Dr Keith L. McLaughlin
PO Box 1620
La Jolla CA 92038-1620

Sierra Geophysics, Inc. 2
ATTN: Dr R. Hart and Dr G. Mellman
11255 Kirkland Way
Kirkland WA 98033

SRI International 1
ATTN: Dr A. Florence
333 Ravensworth Avenue
Menlo Park CA 94025

Teledyne Industries, Inc. 1
Teledyne Geotech Alexandria Laboratories
ATTN: Mr W. Rivers
314 Montgomery Street
Alexandria VA 22314-1581

Woodward-Clyde Consultants 1
ATTN: Dr L. Burdick
PO Box 93254
Pasadena CA 91109-3254

NON-US RECIPIENTS

Ministry of Defense 1
ATTN: Mr Peter Marshall
Blacknest, Brimpton
Reading, FG7-4RS
United Kingdom

National Defense Research Institute 1
ATTN: Dr Ola Dahlman
Stockholm 80
Sweden

NTNF/NORSAR 1
ATTN: Dr Frode Ringdal
PO Box 51
N-2007 Kjeller
Norway

University of Cambridge, Bullard Laboratories 1
ATTN: Dr Keith Priestley
Department of Earth Sciences
Madingley Rise, Madingley Road
Cambridge, CB3 OEZ
United Kingdom

OTHER DISTRIBUTION

To be determined by the project office 9

TOTAL 80